DE-FG26-98FT40113-1

Catalysts for High Cetane Ethers as Diesel Fuels

Kamil Klier, Richard G. Herman, Heock-Hoi Kwon,
Robert A. Hunsicker, Andrew P. Butler, and Scott J. Bollinger

Zettlemoyer Center for Surface Studies
and Department of Chemistry
Sinclair Laboratory, 7 Asa Drive
Lehigh University
Bethlehem, Pennsylvania 18015

Annual Technical Progress Report
for
September 1, 1998-August 31, 1999

Submitted to the

National Energy Technology Laboratory
Pittsburgh, PA

Catalysts for High Cetane Ethers as Diesel Fuels

Disclaimer

Catalysts for High Cetane Ethers as Diesel Fuels

ABSTRACT

A tungstena-zirconia (WZ) catalyst has been investigated for coupling alcohols to unsymmetrical ethers and compared with earlier studied sulfated-zirconia (SZ) and Nafion-H catalysts. In all cases, the ether synthesis mechanism is a dual site S_N2 process involving competitive adsorption of reactants on proximal acid sites. At low reaction temperatures, methylisobutylether (MIBE) is the predominant product. However, at temperatures >135°C the WZ catalyst is very good for dehydration of isobutanol to isobutene. The surface acid sites were diagnosed by high resolution X-ray photoelectron spectroscopy (XPS) of N 1s shifts after adsorption of amines. Using pyridine, ethylenediamine, and triethylamine, it is shown that WZ has heterogeneous strong Brønsted acid sites. Theoretical study located the transition state and accounted well for XPS core-level shifts upon surface acid-base interactions. While computations have not been carried out with WZ, it is shown that the SZ catalyst is a slightly stronger acid than CF_3SO_3H (a model for Nafion-H) by 1.3-1.4 kcal/mol.

Catalysts for High Cetane Ethers as Diesel Fuels

TABLE OF CONTENTS

INTRODUCTION

Dehydrocondensation of two different alcohols takes place over solid acid catalysts either as a concerted S_N2 reaction [1-6] or as a two-step, less efficient process involving carbenium chemistry [7]. The distinction between the two pathways was determined in this laboratory by ^{18}O retention [2,4], chirality inversion [2,5], and structure of the product isomers [2,3]. Side reactions resulted in symmetrical ethers and olefins *via* dehydration of the C_2+ alcohols, in particular branched alcohols.

Over sulfonic acid Nafion-H resin, it was shown by us that methanol (MeOH) and isobutanol (i-BuOH) react fairly selectively to form methyl isobutyl ether (MIBE) from MeOH/i-BuOH = 1 at 0.1 MPa [2] and 2 at ≈1.35 MPa [6,8] at temperatures between 87 and 117°C by a dominant S_N2 reaction pathway [2]. Oxide catalysts tend to require higher reaction temperatures to achieve appreciable conversions and to catalyze the formations of hydrocarbons, e.g. isobutene, rather than ethers [1].

The objective of this research is to develop scientific background of catalysts and processes for technological advancement in the production of high cetane ethers from alcohols and olefins for use as premium diesel fuels. This involves the goals of synthesizing dual-site and ternary-site strong acid heterogeneous catalysts for activating and coupling alcohols to form ethers. The catalysts need to be selective, operate under mild reaction conditions, and economically produce diesel fuels and additives that have high cetane numbers. This is being achieved by preparing, characterizing, and testing solid acid catalysts, and both experimental and computational methodologies are being employed to delineate the active sites.

In this report, we summarize the first-year study of the catalyst formation, activity, selectivity, kinetics, and nature of active sites in the tungstena-zirconia (WZ) system that had been explored for hydrocarbon isomerizations by Santiesteban et al. [9] at Mobil Technology Co. and has now proven to be active for ether synthesis from alcohols in our work. The specific reaction is that of MeOH + i-BuOH, which gives rise at low temperature ($\leq 127°C$), in order of selectivities and abundances, to methyl-isobutyl ether (MIBE) > isobutene (IB) > isooctene (IO) > dimethylether (DME) >> methyl-tertiarybutyl ether (MTBE).

EXPERIMENTAL PROCEDURES

Catalyst Preparation. The WZ catalyst was prepared according to the procedure described elsewhere for a refluxed, impregnated (R/IM) catalyst [9]. Hydrous zirconia was first prepared, which was thereafter calcined to form ZrO_2. This preparation was carried out by added aqueous 10 M NH_4OH dropwise to a stirred $ZrOCl_2$ aqueous solution to precipitate the hydrous zirconia (final pH ≈9). After filtering, the solid was washed with distilled water and dried overnight at 95°C. The solid was reslurried in excess water, the pH adjusted to ≈9.0 with 10 M NH_4OH, and refluxed overnight. After cooling, the solid was filtered, washed with water, and dried overnight at 95°C. The $Zr(OH)_4$ was then impregnated with an ammonium metatungstate $[(NH_4)_6H_2W_{12}O_{40}\bullet xH_2O]$ solution, air-dried at 95°C, and calcined at 825°C for 3 hr. This gave a solid containing nominal 15 wt% W loading and a surface area of 69 m^2/g after calcination, of similar properties as the Mobil Technology Co. preparation with 16.9 wt% tungsten and area of 62 m^2/g [9].

Catalyst Testing. The alcohol coupling reaction was carried out in a downflow stainless steel tubular reactor operated in the differential regime, as described in our earlier study [6]. Typically, 1 g of catalyst diluted with approximately 5 ml of 0.8 mm Pyrex beads was placed in the middle of the reactor between plugs of Pyrex wool. The reactor void volume below and above the catalyst bed was filled with 5 mm Pyrex beads. A J-type thermocouple was inserted into the top of the catalyst bed using an axial stainless steel thermowell.

The reaction rates were typically measured at temperatures between 127°C and 150°C. A mixture of 17.8 vol% N_2 in He (Airgas Northeast, Inc.) was used as a carrier gas. The gas flow rate was controlled using a calibrated mass flow meter (Union Carbide, Model FM-4550). The reactants, methanol and isobutanol (99.9+%, Alfa), were fed separately as liquids to heated lines leading to the inlet port at the top of the reactor using two metering pumps (ISCO, Model 314). The reactants were vaporized in a preheated section of the reactor as they were mixed with the carrier gas before reaching the catalyst bed. The furnace had three heating zones, which provided for very good temperature control. The reactor pressure was controlled by a MightyMite back pressure regulator.

The exit gas stream from the reactor was analyzed by using an on-line Hewlett-Packard gas chromatograph (Model 5890, Series II), which was equipped with automated heated sampling valves. Product analyses were achieved with a Cpsil-5CB capillary column (Chrompack) using a thermal conductivity detector. No dehydration of alcohols was observed over a bed containing only Pyrex beads nor on the reactor walls at temperatures up to 150°C. Steady state activities over the catalysts were achieved within 2 hr of initiating

alcohol injection and after changing the reactor temperature and alcohol feed rate. The catalyst performance was steady over a few hundred hours of testing. For kinetic studies, the total conversion was kept at less than 5% at 127°C and approximately 10% at 150°C. In this range, the system performs as a differential reactor.

Catalyst Characterization by Optical Spectroscopy. All measurements were made with a computer-controlled, scanning, double-beam Cary 5E spectrophotometer (Varian Instruments, Inc.) with diffuse reflectance accessory and extended sample chamber. The integrating sphere was coated with polytetrafluoroethylene (PTFE).

Spectral data were stored on a PC disk and transformed using the Kubelka-Munk relation before being plotted. The diffuse reflectance theory yields quantitative results [10-12] for low absorbing, semi-infinite samples based on the Kubelka-Munk relation, i.e.

$$K/S = (1 - R_\infty)^2 / 2R_\infty, \qquad (1)$$

where K = the absorption coefficient of the sample, S = the scattering coefficient of the sample, and R_∞ = the reflectance of the sample. Where needed, corrections at high absorbances are made [12]. The reflectances of the samples were measured between 4,500 and 50,000 cm^{-1}. The two spectral regions of principal interest are the NIR region between 4,500 and 8,000 cm^{-1} and the UV region between 10,000 and 50,000 cm^{-1}. The NIR region contains vibrational combination bands and overtones of hydrogen-containing species, e.g. hydroxyl groups, which is useful for quantitative analysis of materials with low electronic spectral background. The UV region includes electronic spectra and was used to characterize the optical band edges of the samples.

The surface-doped zirconia samples were dried at 115°C for 24 hr in a furnace, after

which they were removed and allowed to cool in a positive-pressure, nitrogen-filled glove bag or box. The samples were then transferred into diffuse reflectance cells having 1 mm thick 2 cm radius circular Suprasil windows. The cells were closed using a conical rubber stopper and sealed with Mylar film.

Catalyst Characterization by XPS. X-Ray photoelectron spectroscopy (XPS) analyses of the WZ catalysts before and after adsorption of amines were carried out using the Scienta ESCA-300 high resolution photoelectron spectrometer at Lehigh University [13]. This instrument utilizes a rotating Al Kα anode to generate an unpolarized 7.6 KW X-ray flux ($h\nu$ = 1486.8 eV), which is monochromatized by seven toroidally bent quartz crystals. The detector system, consisting of a 300 mm mean radius hemispherical electron energy analyzer and a multichannel plate detector, provided an overall energy resolution of 0.27 eV, as determined by the Fermi level edge from Ag at room temperature. The detector's high sensitivity and energy resolution allows for the analysis of insulated samples. To improve the quality of resolution for non-conducting materials, a Scienta hot filament flood gun with an energy range of 0-10 eV is available to supply electrons for charge compensation.

For XPS analysis, the ZrO_2 and the W/Z catalyst were each pressed into pellet form on top of a rectangular piece of tin using a hydraulic ram press. The pellet was then secured onto an ESCA analysis stub by clamping the edges of the tin piece to the stub with screws. The stub with the sample was inserted into the fast entry chamber of the Scienta instrument and evacuated to pressures < 1 x 10^{-6} Torr. The stub was then transferred into the analysis chamber where the surface of the sample was scraped *in situ* (using a SiC edge) to remove any adsorbed impurities.

Both the survey and the high-resolution scans were performed on the clean ZrO_2 and W/Z surfaces, with the pressure in the analysis chamber on the order of 5×10^{-9} Torr. Survey scans were conducted with 300 eV pass energy, an incremental step size of 1 eV, and a 0.8 mm slit width. Scans of Zr 3d, O 1s, C 1s, W 4f, and N 1s spectral regions were conducted in a high resolution mode with 150 eV pass energy, an incremental step size of 0.05 eV, and a 0.8 mm slit width. The pass energy refers to the energy to which the kinetic energy of the emitted photoelectrons is retarded by a retardation voltage for detection by the analyzer. The step size in turn refers to the energy step between each sweep of the retardation voltage. The slit width refers to the width of the slit located at the entrance of the detector. A larger slit width provides increased photoemission intensity with poorer resolution. Because the W/Z catalyst was non-conducting, a hot filament gun set at 1.3 eV was applied during the analysis to supply electrons for charge compensation and improve the resolution.

The adsorption of amines onto dehydrated W/Z (and Nafion-H microsaddles) was performed on a separate glass vacuum/adsorption system. Each dehydrated powdered sample was transferred into a glass reaction tube, which was connected *via* a Cajon ultra Torr tube connector to a port on the vacuum manifold having a Teflon/glass stopcock. The sample was evacuated to pressures on the order of 10^{-3} Torr prior to the adsorption of the amines. The amines were purified by a freeze/thaw technique using liquid nitrogen as coolant. The catalysts were exposed to the purified amines at room temperature and 15 Torr for 30 min. The catalysts were again evacuated to 10^{-3} Torr following the exposure. The adsorption system allowed for heating the catalyst before and/or after the adsorption

treatment, where the latter provided for desorption of loosely adsorbed amines.

After the adsorption/evacuation treatment, the glass connecting tube between the stopcock and the vacuum system was break-opened, and the evacuated tube was moved to a nitrogen-filled glove bag or glove box. Opening the stopcock filled the tube with nitrogen, after which the tube was removed from the Cajon tubing connector, and the powdered sample was mounted on an ESCA analysis stub with the use of double sided sticking tape. The surface of the mounted sample was smoothed by using pressure applied from a smooth spatula. The prepared stub was transferred in a nitrogen-filled desiccator from the glove box or bag to a glove bag attached to the entrance port of the Scienta ESCA 300 fast entry chamber. The chamber was brought to atmospheric pressure with nitrogen and the sample was transferred from the glove bag to the fast entry chamber. After sealing the fast entry chamber, it was evacuated to approximately 1×10^{-6} Torr, after which the sample was moved into the analytical chamber, which maintained a vacuum of approximately 10^{-9} Torr.

CATALYTIC RESULTS FOR THE WO_3/ZrO_2 CATALYST

Dehydration of Mixed Alcohols. A kinetic study was carried out with mixtures of methanol and isobutanol at a total reaction pressure of 1.36 MPa. In these studies, the partial pressure of one alcohol was maintained constant while the partial pressure of the other alcohol was varied. This allowed for determination of reaction rates and kinetic parameters for isobutanol dehydration to form isobutene (IB) and coupling reactions to form dimethylether (DME), diisobutylether (DIBE), and methylisobutylether (MIBE) using Equations (2)-(5).

$$\nu_{DME} = k_1 K_M^2 p_M^2 / (1 + K_M p_M + K_B p_B)^2 \quad (2)$$

$$\nu_{DIBE} = k_2 K_B^2 p_B^2 / (1 + K_M p_M + K_B p_B)^2 \quad (3)$$

$$\nu_{IB} = k_3 K_B p_B / (1 + K_M p_M + K_B p_B)^2 \quad (4)$$

$$\nu_{MIBE} = k_4 K_M p_M K_B p_B / (1 + K_M p_M + K_B p_B)^2 \quad (5)$$

In these equations utilized for determining the formation rates (ν_i) of the products, p_M is the partial pressure of methanol, p_B is the partial pressure of isobutanol, the k_n values are the kinetic constants, and the K_n values are the adsorption equilibrium constants.

Results obtained at reaction temperatures of 127°C and 176°C are shown in Figure 1, which represents MIBE formation rates as a function of partial pressure of each reactant while keeping the pressure of the second alcohol constant. Symbols represent experimental data at 150°C and the full lines are theoretical curves based on Langmuir-Hinshelwood kinetics as described in Nunan et al. [6]. The MIBE formation rates show maxima in the dependence on partial pressures of both alcohols at both reaction temperatures, which implies optimum regime for the MIBE synthesis by either alcohol. The kinetic and adsorption equilibrium constants were obtained by fitting Equation (5) given above.

Figure 2 shows examples of using the linear forms of the rate laws, where (a) the partial pressure of isobutanol was maintained constant at 13 kPa while varying the methanol partial pressure and (b) methanol was maintained constant at 23 kPa while varying the isobutanol partial pressure. These linear plots yield the slopes and intercepts for experiments in which pM and pB were separately varied. The ratio of the intercept to the slope in each linear plot provided $(1 + K_B p_B) / K_M$ and $(1 + K_M p_M) / K_B$, respectively. Since p_M and p_B were set as constants, K_M and K_B could be determined unambiguously.

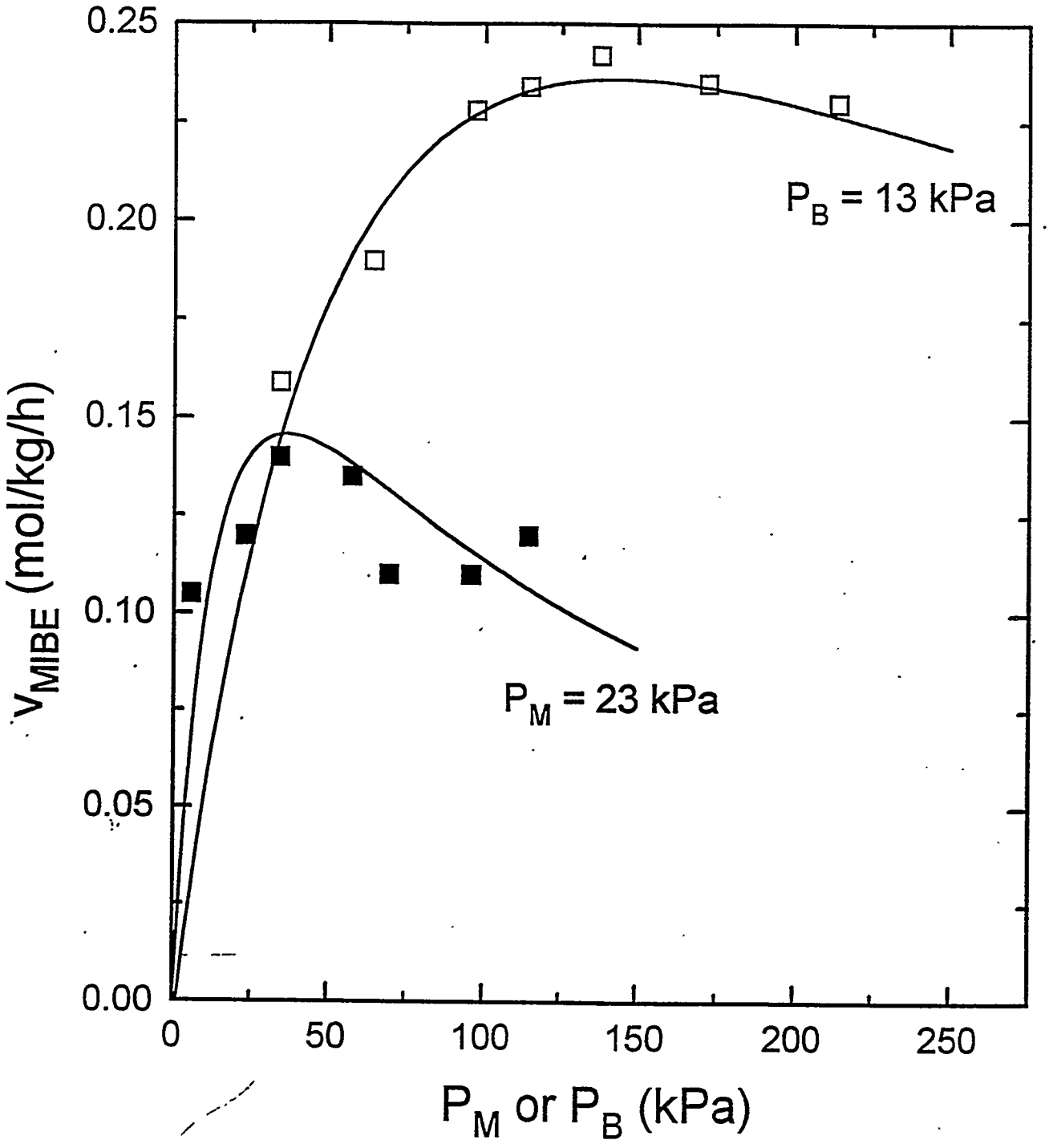

Figure 1. Rates of MIBE formation from mixtures of methanol and isobutanol as a function of partial pressure of methanol, p_M, while keeping partial pressure of isobutanol, p_B, constant at 13 kPa (□), and p_B with constant p_M at 23 kPa (■) over 1.0 g of the tungstena/zirconia (WZ) catalyst. The reaction conditions were 150°C, p_{total} =1360 kPa, and 18.7% N_2/He + alcohol feed rate of 125 mol/kg catalyst/h. Squares are experimental data and full lines are theoretical curves obtained by using Eq. (5) for the dependence of v_{MIBE} on p_M and p_B with k_4 = 3.1 mol/kg/h, K_M = 0.010 kPa^{-1}, and K_B = 0.034 kPa^{-1}.

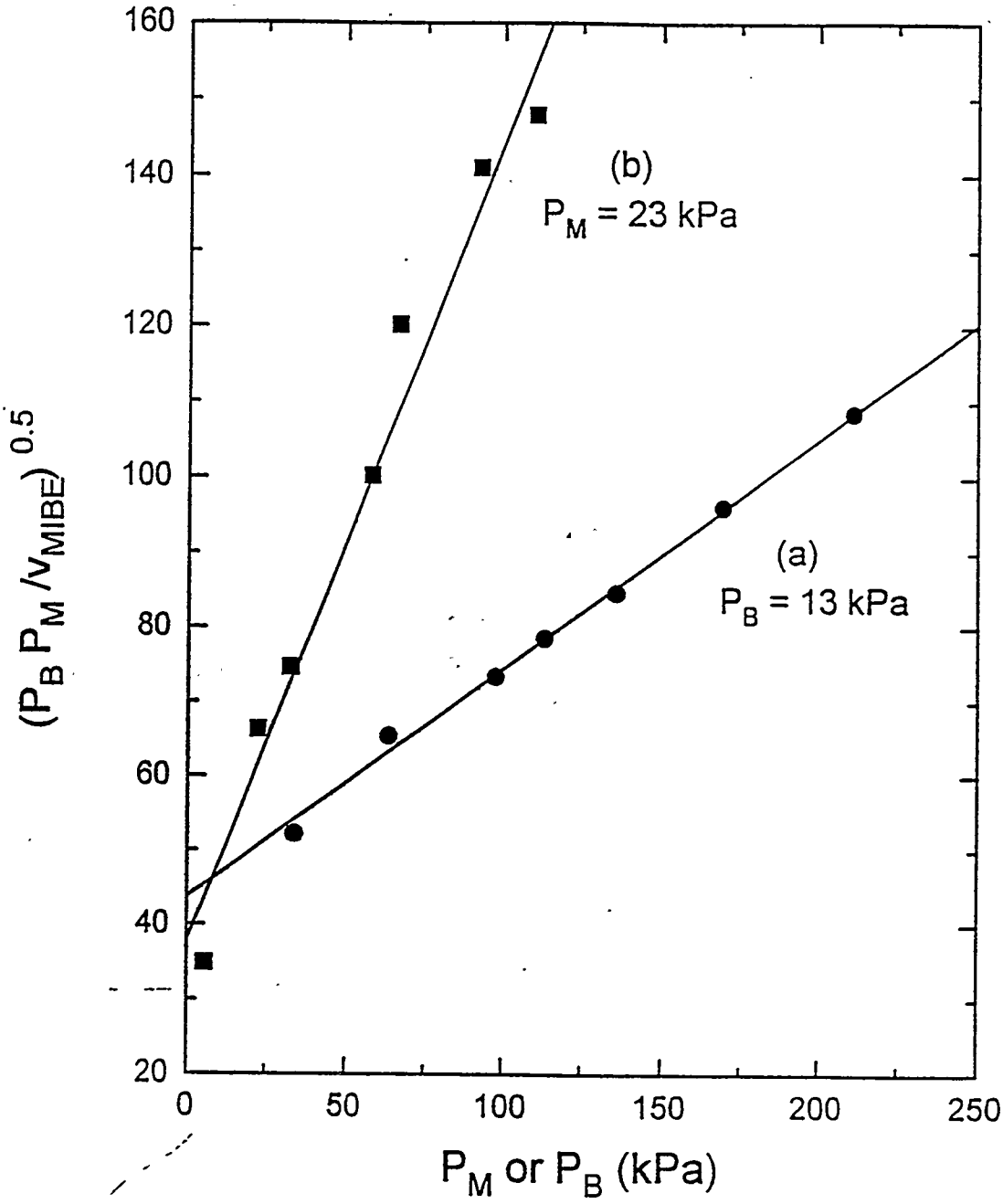

Figure 2. Langmuir-Hinshelwood linear plot for the dehydration of methanol and isobutanol to MIBE over 1.0 g tungstena/zirconia catalyst at 150°C, p_{total} = 1360 kPa, and 18.7% N_2/He + alcohol feed rate of 125 mol/kg catalyst/h. The slope and intercept give combinations of rate and equilibrium constants (a) $\sqrt{(K_M/(k_4K_B))} = 0.309$ and $(1 + K_b p_B)\sqrt{(k_4K_MK_B)} = 43.8$, with p_B = 13 kPa and varying the partial pressure of methanol p_M, and (b) $\sqrt{(K_B/(k_4K_M))} = 1.05$ and $(1 + K_m p_M)\sqrt{(k_4K_MK_B)} = 37.95$, with p_M = 23 kPa and varying the partial pressure of methanol p_B. k_4 is in mol/kg catalyst/h and K_M and K_B are in kPa^{-1} .

The kinetic and adsorption equilibrium constants were $k_4 = 3.1$ mol/kg/h, $K_M = 0.010$ kPa^{-1}, and $K_B = 0.034$ kPa^{-1} at 150°C. At 127°C, theoretical curves with $k_4 = 0.93$ mol/kg/h, $K_M = 0.011$ kPa^{-1}, and $K_B = 0.039$ kPa^{-1} successfully fitted the experimental data. The ratio of K_B/K_M was 3.4 at 150°C and 3.5 at 127°C, respectively, implying that isobutanol adsorbs more strongly to the active sites on the surface than methanol. Under similar reaction conditions (127°C and 1340 kPa), Nafion-H was reported to have the following constants: $k_4 = 2.78$ mol/kg/h, $K_M = 0.0137$ kPa^{-1}, $K_B = 0.0243$ kPa^{-1}, and $K_B/K_M = 1.8$ [6]. Although the constants are of the same order of magnitude, Nafion H turned out to be approximately 2.4 times more active for MIBE production than the present tungstena/zirconia catalyst.

With the rate constant obtained at 150 °C and activation energy (discussed later in this report) for MIBE formation, k_4 at 127°C could be determined from the Arrhenius rate expression, $k_4 = A \exp(-E_a/RT)$. The k_4 value was determined to be 1.04 mol/kg/h with a pre-exponential factor of $A = 5.7 \times 10^8$. This value of k_4 is very close to that determined from the separate experiment described above. In addition, the equilibrium constants K_B and K_M could also be determined from the data for DME and IB formation by using the linearized forms of Equations (2) and (4). The resulting linear plots were shown in Figure 3, yielding $K_M = 0.015$ kPa^{-1} and $K_B = 0.037$ kPa^{-1} (and $k_4 = 2.7$ mol/kg/h). The theoretical curves with the equilibrium and kinetic constants so obtained deviated appreciably from the experimental data and did not fit the experimental data as well as those shown in Figure 1. However, correct trends were predicted, and the values of K_B and K_M were not too different from those determined from the MIBE experiment, as shown in Figure 1 with derived values of K_B and K_M of 0.034 and 0.010 kPa^{-1}, respectively.

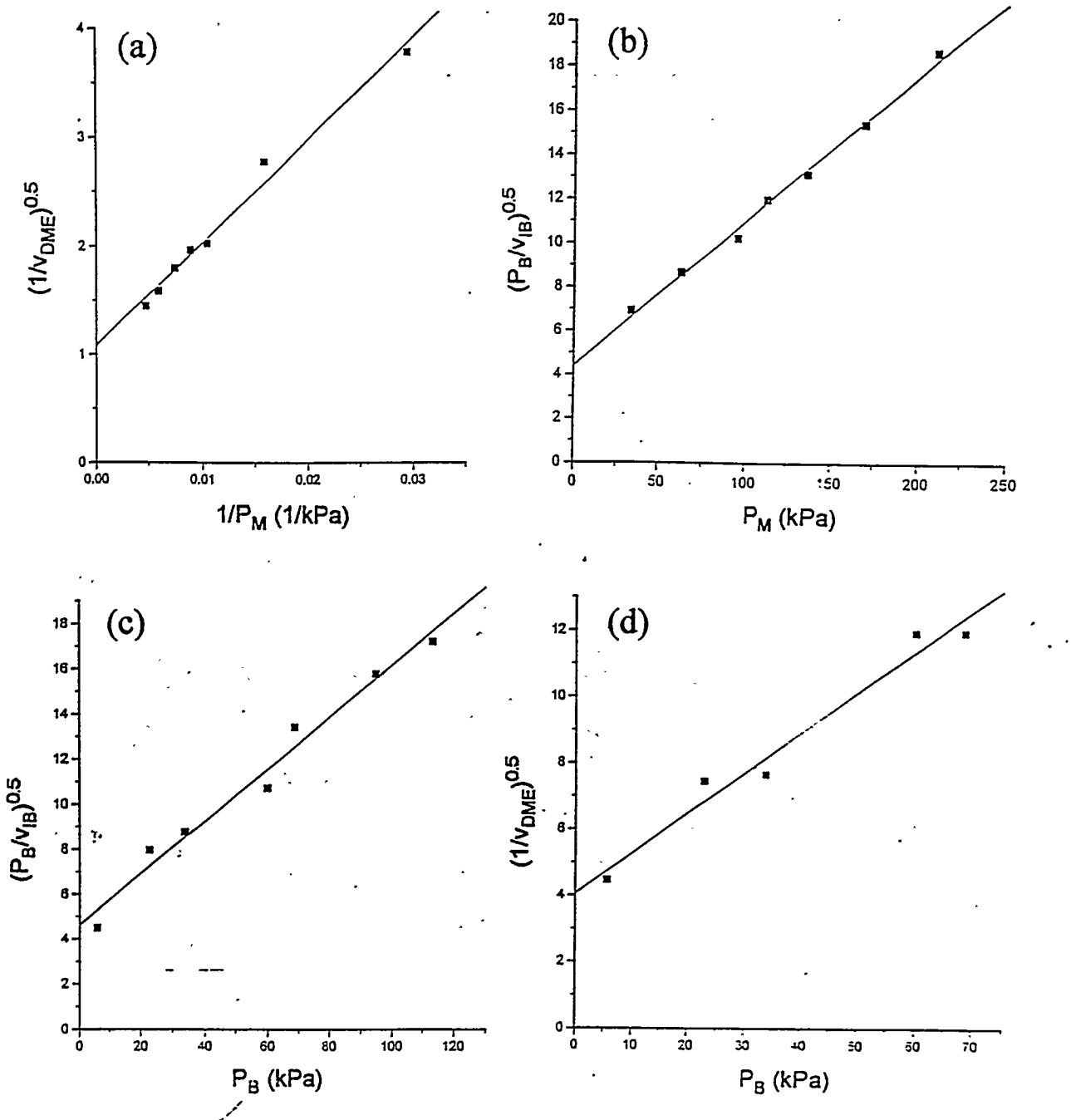

Figure 3. Langmuir-Hinshelwood linear plot for the dehydration of methanol and isobutanol to MIBE over 1.0 g tungstena/zirconia catalyst at 150°C, p_{total} = 1360 kPa, and 18.7% N_2/He + alcohol feed rate of 125 mol/kg catalyst/h. The slope and intercept give combinations of rate and equilibrium constants (a) $\sqrt{k_1} = 1.08$ and $(1 + K_B p_B) / \sqrt{(k_1 K_M^2)} = 94.7$ and (b) $K_M \sqrt{(k_3 K_B)} = 0.066$ and $(1 + K_b p_B) / \sqrt{(k_3 K_B)} = 4.39$ where p_B = 13 kPa and the partial pressure of methanol p_M was varied, and (c) $\sqrt{(K_B/k_3)} = 0.116$ and $(1 + K_m p_M) / \sqrt{(k_3 K_B)} = 4.61$ and (d) $K_B / \sqrt{(k_3 K_M p_M)} = 0.122$ and $(1 + K_m p_M) / \sqrt{(k_1 K_M p_M)} = 4.04$, where p_M = 23 kPa and the partial pressure of methanol p_B was varied. k is in units of mol/kg catalyst/h and K_M and K_B are in units of kPa^{-1}.

Dehydration of Individual Alcohols. Experiments were also carried out using only one of the alcohols as a reactant at 127°C and p_{total} = 1360 kPa. In methanol dehydration in the absence of isobutanol, DME was the only reaction product observed, and the formation rate was leveling off at high methanol pressures (Figure 4). For isobutanol dehydration, isobutene and isooctene were the major products. The cis- and trans-2-butenes were observed as minor products, but no diisobutylether (DIBE), which is one of the significant products over Nafion H, was detected. The rates of formation of the major products formed from isobutanol are shown in Figure 5. Using the same graphical analysis methods as previously described, the plots shown in Figure 6 were obtained. The kinetic and equilibrium constants from this analysis of the reactions of the individual alcohols were determined to be in the same order of magnitude (K_M = 0.014-0.047 kPa^{-1} and K_B = 0.0196 kPa^{-1}). Although the K_M value from MIBE synthesis with mixed alcohols was within the range of the value of K_M obtained from the methonol-only experiment, the K_M value varied depending on p_M, implying failure of the Langmuir-Hinshelwood kinetic analysis based on Equation (2). Further data analysis will be carried out to obtain an explanation and/or a better kinetic equation.

Temperature Effect on Selectivity. In order to elucidate the effect of temperature on product selectivity over the tungstena/ zirconia catalyst, the reaction temperature was varied between 127°C and 150°C while keeping the total pressure constant at 1360 kPa. The reactant ratio methanol/isobutanol = 2 was maintained. The product selectivity as a function of temperature is shown in Figure 7. At 127°C, MIBE was the dominant product, but at

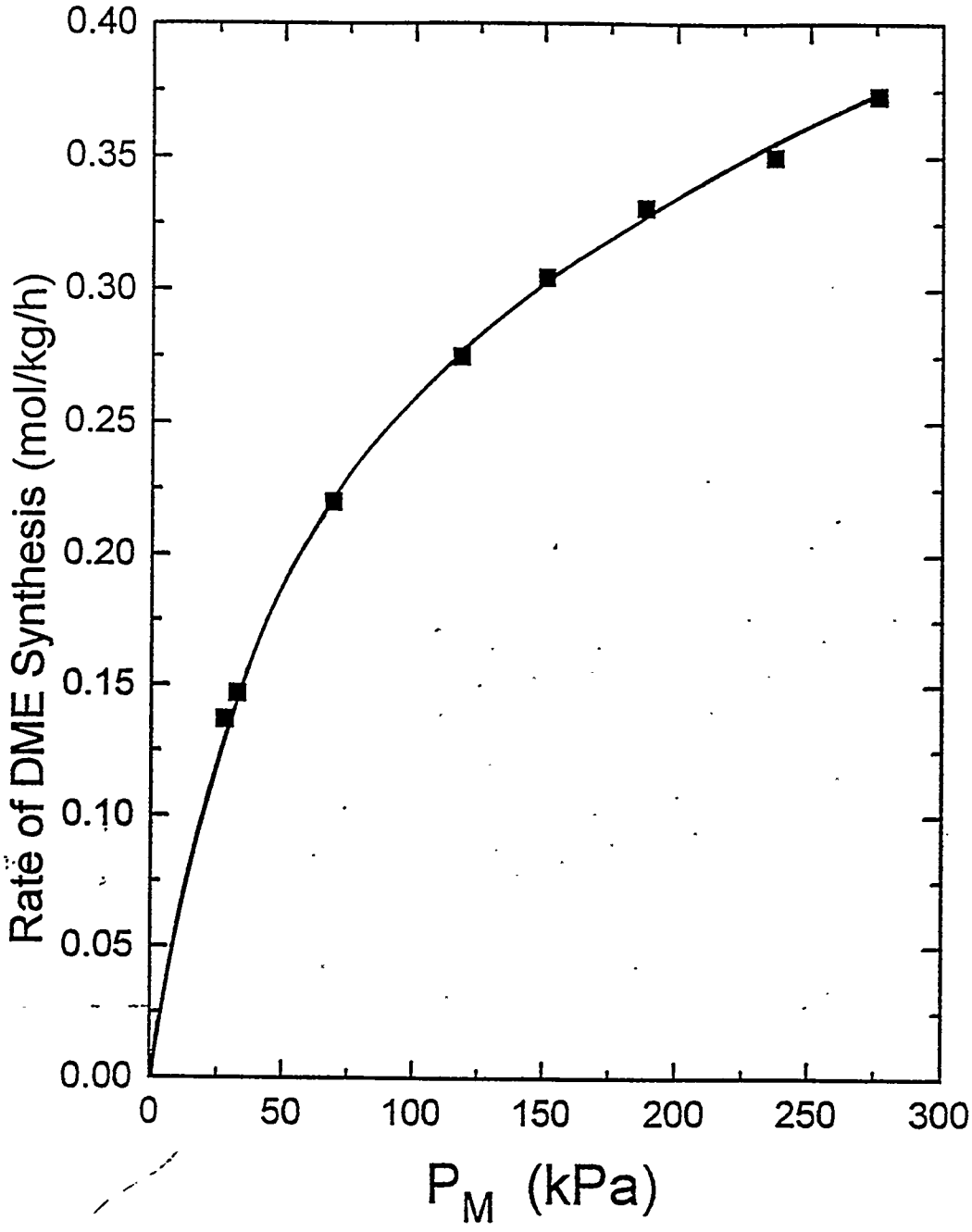

Figure 4. Effect of methanol partial pressure (p_M) on the steady state rate of formation of DME over 1.0 g tungstena/zirconia at 127°C, p_{total} = 1360 kPa, and 18.7% N_2/He + alcohol feed rate of 125 mol/kg catalyst/h.

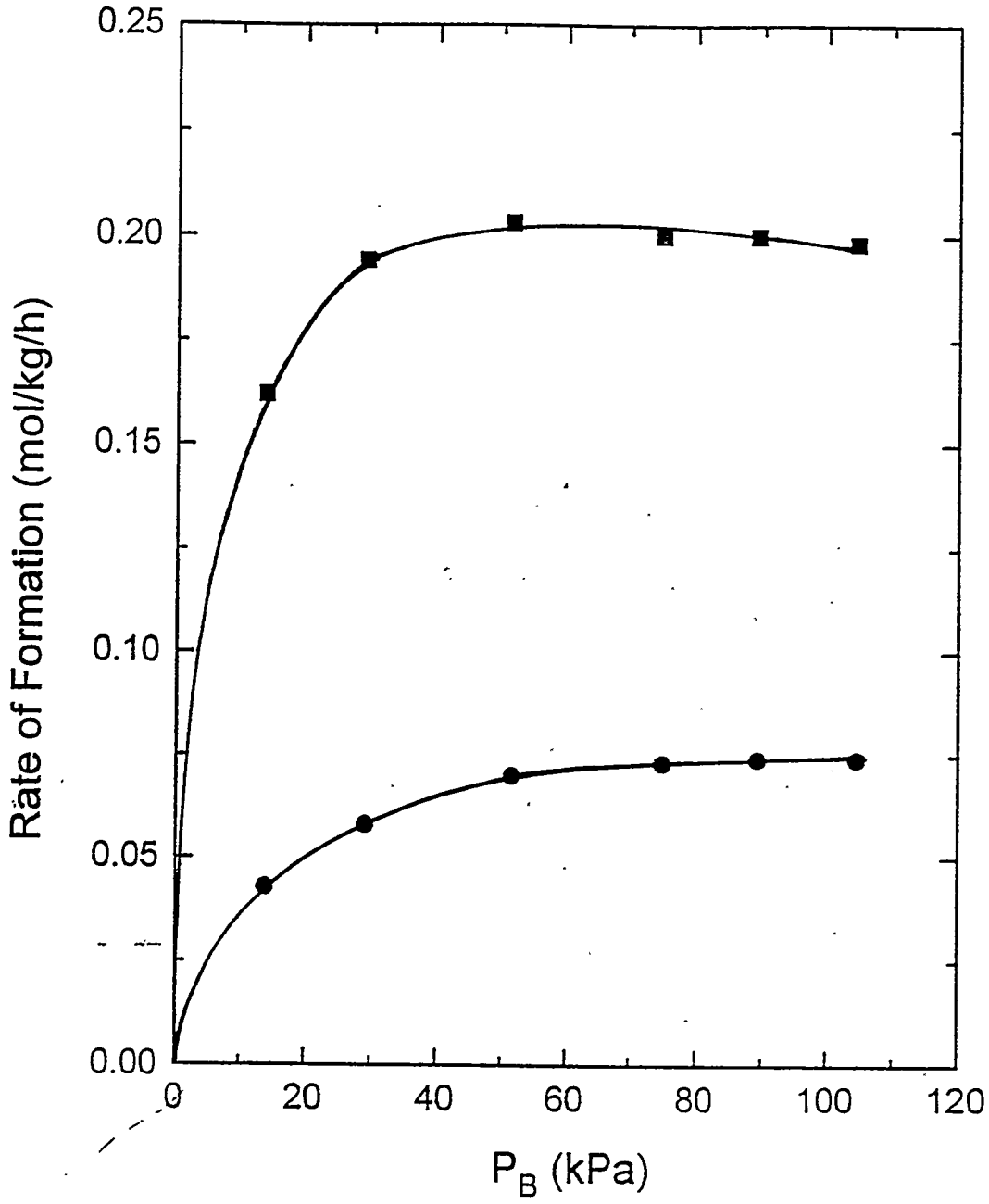

Figure 5. Effect of isobutanol partial pressure (p_B) on the steady state reaction rates for the major products, isobutene (■) and isooctene (●), over 1.0 g tungstena/zirconia at 127°C, p_{total} = 1360 kPa, and 18.7% N_2/He + alcohol feed rate of 125 mol/kg catalyst/h.

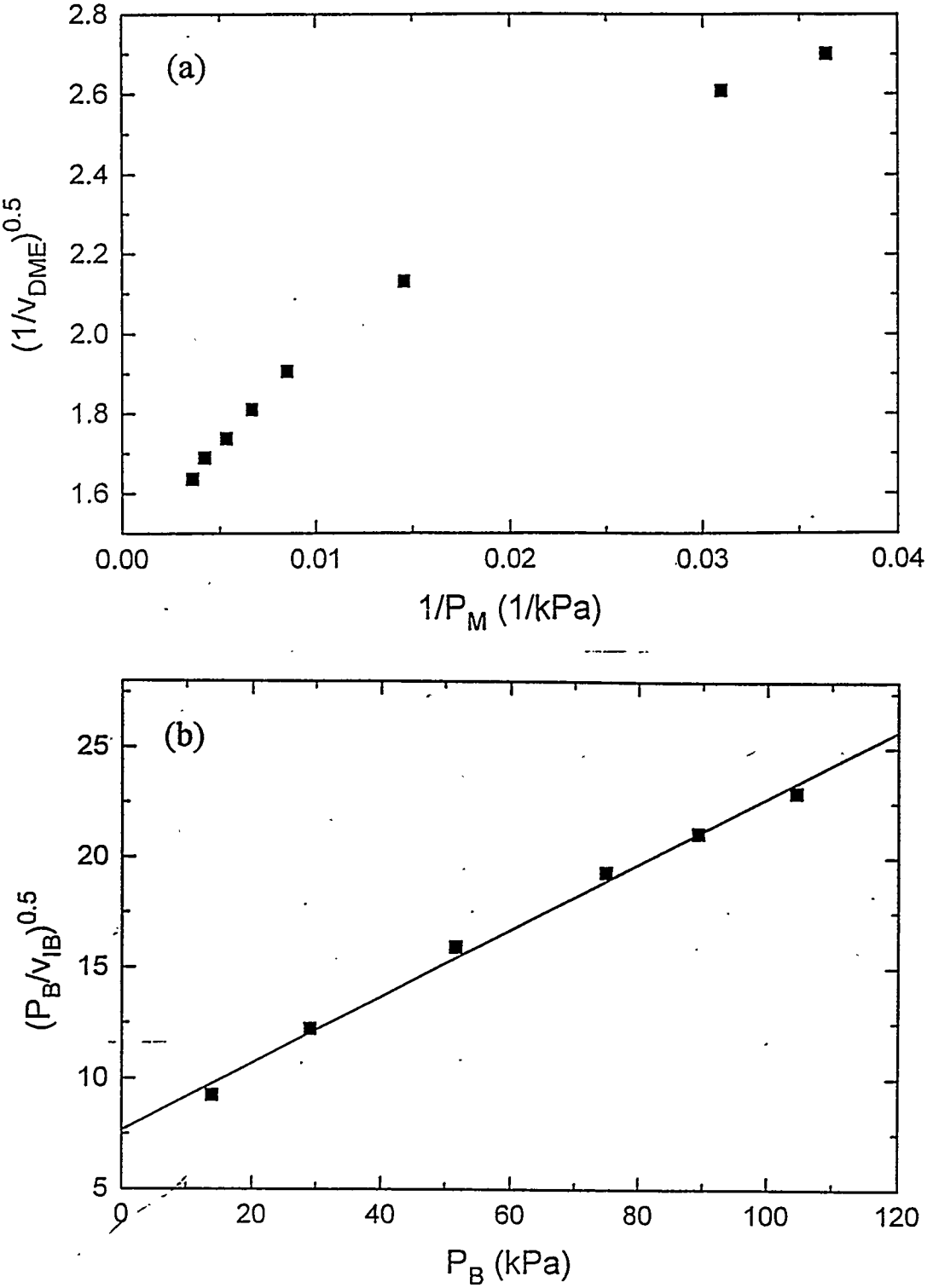

Figure 6. Langmuir-Hinshelwood linear plot for the dehydration of (a) methanol and (b) isobutanol over 1.0 g tungstena/zirconia catalyst at 127°C, p_{total} = 1360 kPa. The slope and intercept give combinations of rate and equilibrium constants (a) $1 / \sqrt{k_1} = 1.25$ for the two highest p_M data points and 2.06 for the two lowest p_M data points and $1 / \sqrt{k_1 K_M} = 91.3$ and 17.8, respectively, and (b) $\sqrt{(1 / (k_3 K_B))} = 7.7$ and $\sqrt{(K_B / k_3)} = 0.15$. k is in units of mol/kg catalyst/h and K_M and K_B are in kPa^{-1} .

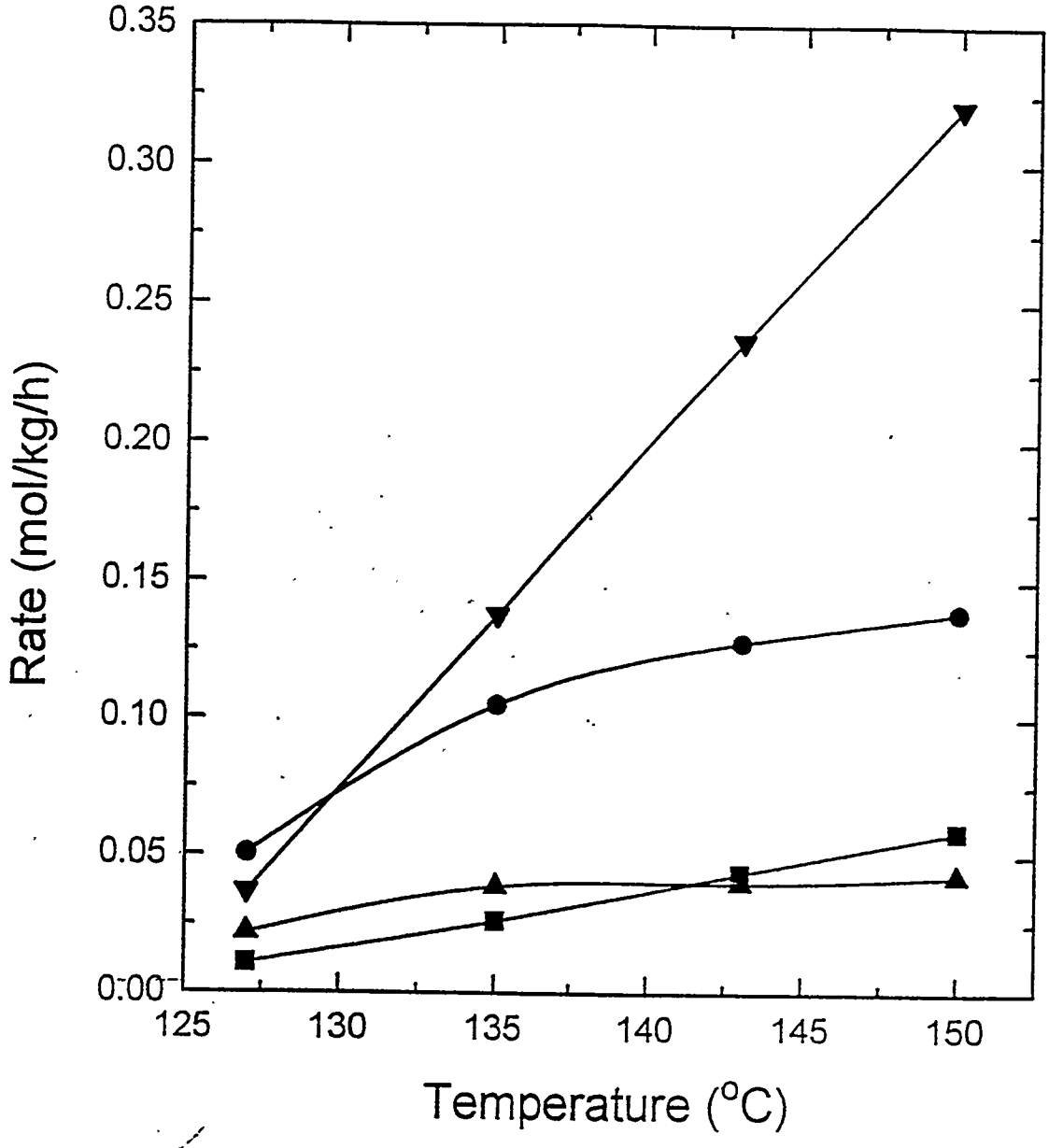

Figure 7. Effect of temperature on the steady state reaction rates of MIBE (●), butenes (▼), octene (▲), and DME (■) over 1.0 g tungstena/zirconia with methanol/isobutanol = 2/1 at p_{total} = 1360 kPa, and 18.7% N_2/He + alcohol feed rate of 125 mol/kg catalyst/h.

higher temperatures (>130°C) butenes predominated. The butenes, octenes, and DME were the next in decreasing order. Increasing the reaction temperature resulted in an increase in the formation of all products, but butenes were the dominant product at 135°C and higher temperatures. MIBE became the second most abundant product. MTBE, an isomer of MIBE, was formed in a smaller amount, typically 5% of the amount of MIBE regardless of reaction temperature. Among butenes, isobutene was the major product, while linear butenes formed between 15 and 25% of the amount of isobutene. Thus, the higher the reaction rate, the larger the quantity of linear butenes that were formed. Among the octenes, 2,5-dimethylhexene was predominant over the entire temperature range, with increasing selectivity to 2,2,4-trimethylpentene as temperature increased.

The apparent activation energy for the formation of individual products was determined from Arrhenius plots, as shown in Figure 8. Apparent activation energies were as follows: 113 ± 8 kJ/mol for DME, 67 ± 17 kJ/mol for MIBE, 121 ± 29 kJ/mol for isobutene, and 38 ± 17 kJ/mol for isooctene. In the case of gel-type Nafion H at 1344 kPa, the values determined were 84.2-87.5 kJ/mol for DME, 84.3 kJ/mol for MIBE, 144.6 kJ/mol for butenes + octenes [8]. In comparison, with a porous Nafion-H MS catalyst at 7600 kPa, the obtained activation energies were 79 kJ/mol for DME, 61 kJ/mol for MIBE, and 227 kJ/mol for isobutene [14]. The activation energies for ether formation are thus lower than the activation energies for olefin formation on both WZ and Nafion-H catalysts.

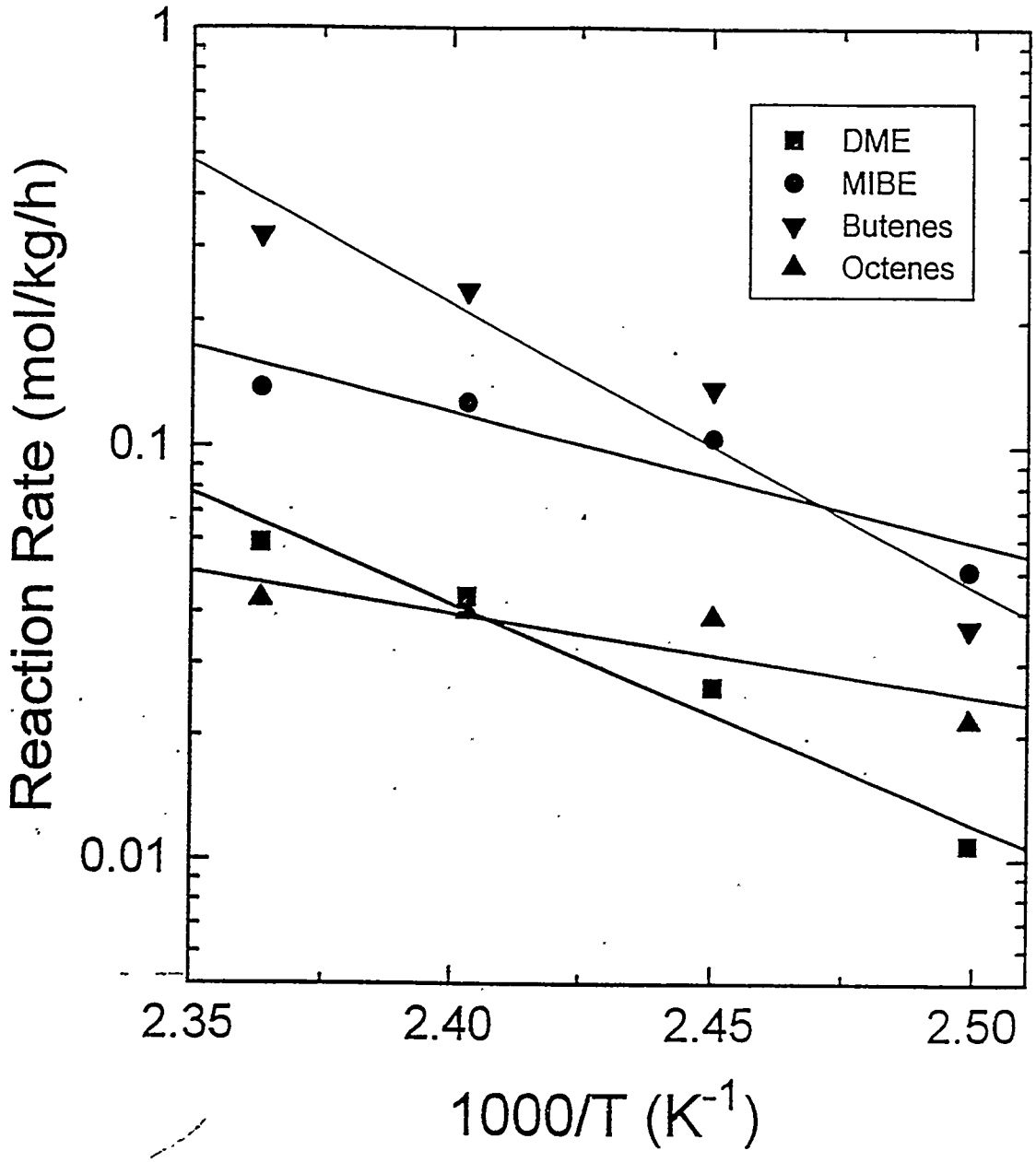

Figure 8. Arrhenius plots of the formation rates of the major products MIBE (●), butenes (▼), octenes (▲), and DME (■) formed over the tungstena/zirconia catalyst with methanol/isobutanol = 2/1 at p_{total} = 1360 kPa, and 18.7% N_2/He + alcohol feed rate of 125 mol/kg catalyst/h.

OPTICAL PROPORTIES OF THE CATALYSTS

Diffuse reflectance studies were carried out in the ultraviolet/visible/near-infrared (UV/Vis/NIR) spectral regions to provide information on the electronic structure, the degree of hydration, and presence of hydroxyl groups of zirconia, tungstena/zirconia, and sulfated zirconia samples.

Spectral Data and Analysis. The optical spectra of the three dehydrated samples were collected over the range of 4,500-50,000 cm^{-1}. The diffuse reflectance spectra (DRS) over this full spectral range are shown in Figure 9. It is clear that the optical properties of the three samples reflect the structure and composition of the catalysts.

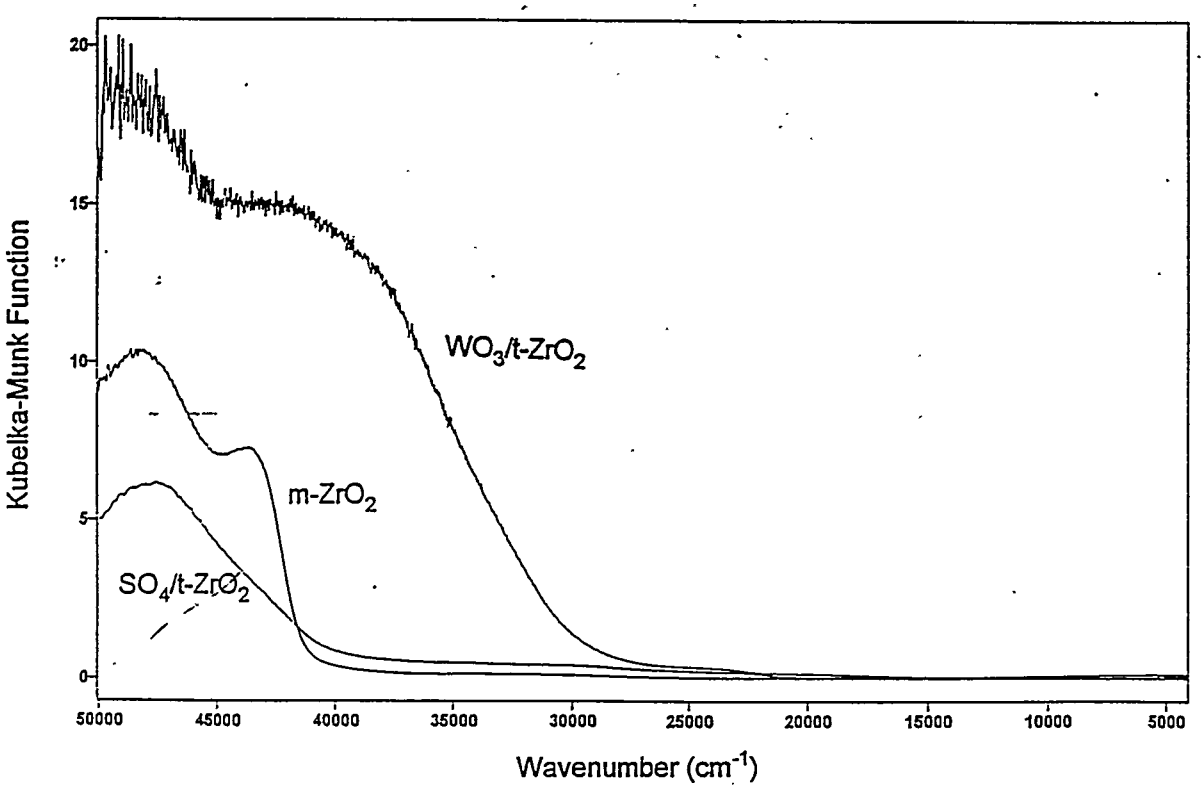

Figure 9. The diffuse reflectance spectra of monoclinic zirconia (m-ZrO_2), tetragonal SO_4-impregnated zirconia (SO_4/t-ZrO_2), and tetragonal WO_3-impregnated zirconia (WO_3/t-ZrO_2) between 4,500 and 50,000 cm^{-1}.

The spectra in the NIR region are shown in Figure 10. For the three samples, the two particular bands of interest in the NIR region are the H_2O ($\nu + \delta$) band at about 5,250 cm^{-1}, which is a combination of stretching and bending modes, and the mixed H_2O (2ν) + OH (2ν) overtone band of the OH stretch at approximately 7,200 cm^{-1}. The former can be used to monitor the degree of dehydration, while the latter can be used to monitor the hydroxyl groups, which are Brønsted acid sites. These groups are present on ZrO_2. Upon sulfating the zirconia, a larger peak at 7159 cm^{-1} was observed, corresponding to an increased number of hydroxyl groups (Brønsted acid sites). Upon tungstating the zirconia, a high optical background was observed and the number of free hydroxyls detected greatly decreased, as indicated by the low intensity of the 7092 cm^{-1} band compared with the ZrO_2 bands.

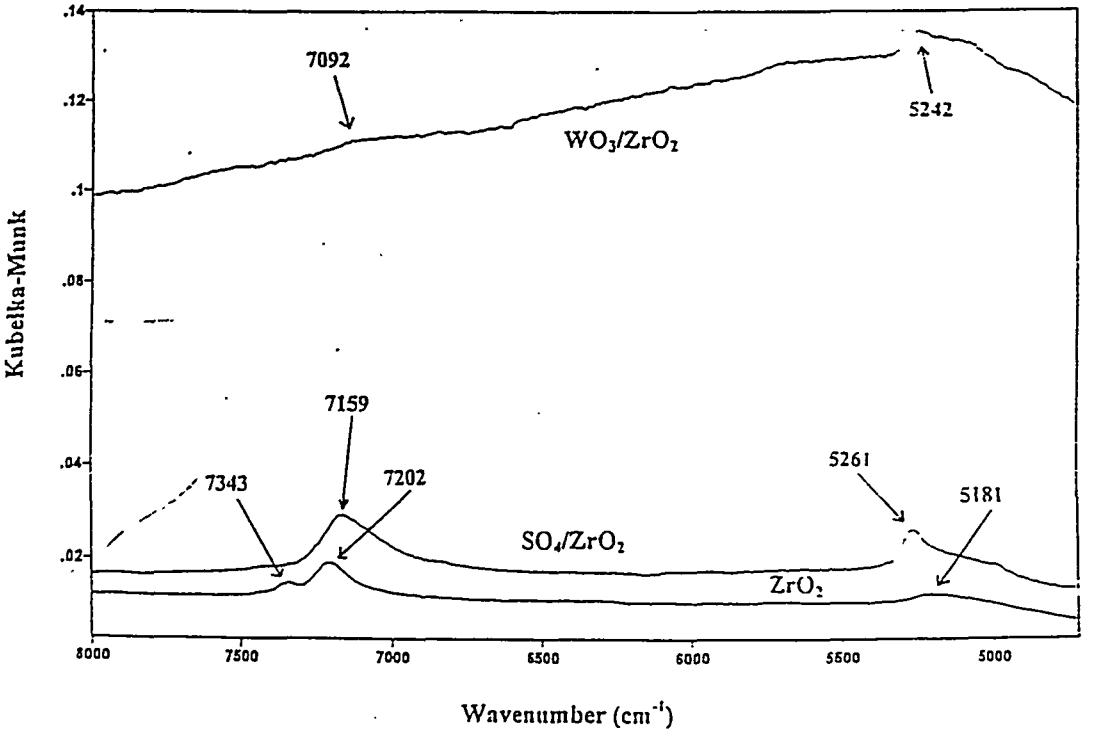

Figure 10. DRS in the NIR region of monoclinic zirconia, tetragonal SO_4-impregnated zirconia, and tetragonal WO_3-impregnated zirconia in the spectral range of 4,500 and 8,000 cm^{-1}. Peak positions are labelled, but accurate calibration needs to be carried out.

The difference spectrum in the OH NIR region of the WO_3/ZrO_2 catalyst was derived for comparison with the distinct spectrum of ZrO_2 that exhibits two peaks. The absorption spectrum for WO_3/ZrO_2 is shown on the same scale as for ZrO_2 in Figure 11. Also shown is the difference spectrum for WO_3/ZrO_2 that was obtained by magnifying the Kubelka-Munk transformed spectra by a factor of 10 and subtracting the background. The diminished intensity of the OH frequencies upon surface impregnation of the zirconia with tungstate indicates bonding of the tungstate species to the surface of the zirconia *via* the surface hydroxyl groups and that it is spread on the surface. There are relatively few hydroxyls present on the tungstated zirconia surface, and those exhibit a shift from ≈7205 cm^{-1} on monoclinic zirconia to *ca.* 7120 cm^{-1} on the tungstated zirconia surface, perhaps arising from low-concentration Brønsted acid sites on the tungstate overlayer.

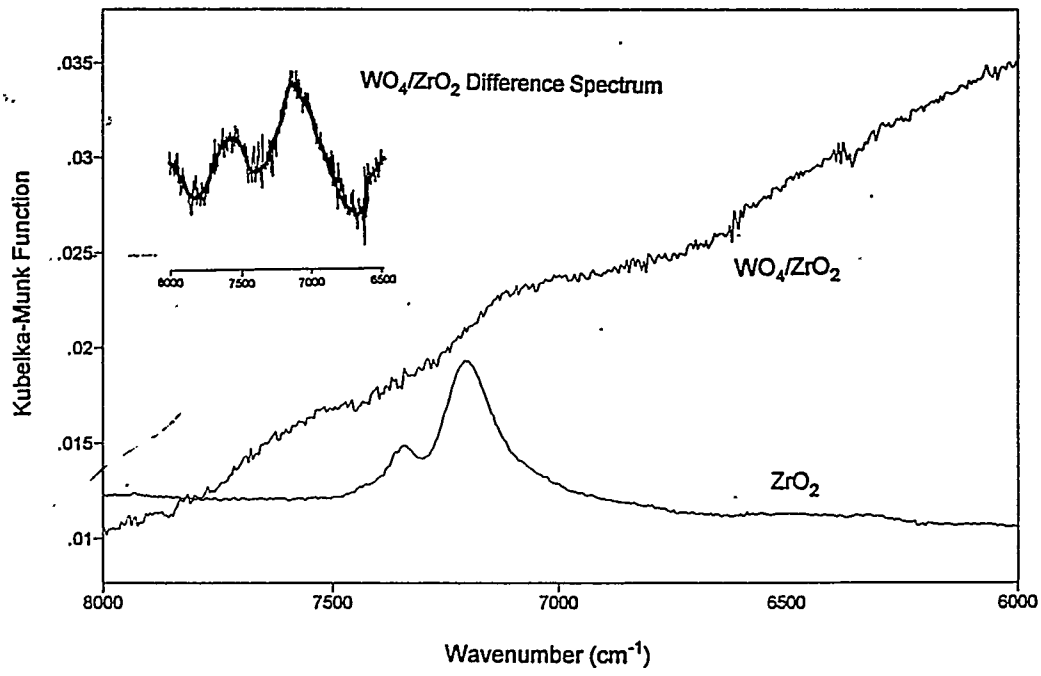

FIGURE 11. The NIR-DRS spectra of the hydroxyl absorption region for monoclinic zirconia and tetragonal tungstated zirconia on the same relative scale, along with the magnified difference spectrum obtained for the latter sample.

The areas of the two bands in the NIR region at about 5,250 cm^{-1} [H_2O ($\nu + \delta$) combination band] and at approximately 7,200 cm^{-1} [mixed H_2O (2ν) + OH (2ν) overtone band] were calculated for each sample by subtracting a linear background and fitting multiple (usually 3-5) Gaussians to the bands. The areas of the Gaussians in the peak were then summed, and the results of the Gaussian fitting are shown in Table 1.

The approximate concentrations of hydroxyls on the three samples were then calculated based on the assumption that the relative intensities of the H_2O ($\nu + \delta$) and H_2O (2ν) bands were in the ratio of 5/1, as in earlier studies [15]. The equation, derived from this work, to calculate the intensity of the OH (2ν) band from the intensities of the mixed H_2O (2ν) + OH (2ν) overtone band and the H_2O ($\nu + \delta$) combination band is

$$I_{[H2O\,(2\nu)+OH\,(2\nu)\,mixed\,band]} = I_{OH\,(2\nu)} + [I_{H2O\,(\nu+\delta)} / 5], \qquad (6)$$

where **I** = the integrated intensity or peak area.

The hydroxyl concentration of the tetragonal zirconia impregnated with surface sulfate was determined in this laboratory [13] using a method of controlled incremental adsorption and desorption of different nitrogen-containing bases. The surface sulfate concentration was found to be 0.55 monolayer. The concentrations of hydroxyls on the tetragonal WO_3-impregnated zirconia and on monoclinic zirconia were calculated by using the known hydroxyl concentration of the tetragonal SO_4-impregnated zirconia, calculated as $I_{OH\,(2\nu)}$ intensities, and Equation 6 given above. The calculated hydroxyl concentrations are given in Table 2. In all cases, the OH surface concentration was determined to be appreciably less than one monolayer.

Table 1. The Gaussian fitting results of the H_2O ($\nu + \delta$) combination bands and the mixed H_2O (2ν) + OH (2ν) overtone bands in the NIR regions of monoclinic zirconia, tetragonal SO_4-impregnated zirconia, and tetragonal WO_3-impregnated zirconia as determined by DRS.

Sample	2ν Bands (H_2O and OH)			H_2O ($\nu + \delta$) Bands		
m-ZrO_2	No. of Gaussian Peaks In Band			No. of Gaussian Peaks In Band		
	Peak	Peak Center	Peak Area	Peak	Peak Center	Peak Area
	1	7424.095	0.0473	1	5364.610	0.0304
	2	7144.920	0.6076	2	5301.622	0.0278
	3	7348.438	0.1703	3	5228.950	0.1210
	4	7208.340	0.6081	4	5158.892	0.0193
	--			5	5129.900	0.2517
	Total Peak Area: 1.4332			Total Peak Area: 0.4502		
WO_3/ t-ZrO_2	No. of Gaussian Peaks In Band			No. of Gaussian Peaks In Band		
	Peak	Peak Center	Peak Area	Peak	Peak Center	Peak Area
	1	7612.789	0.2289	1	5077.164	0.1458
	2	7508.370	0.0415	2	5155.256	0.4088
	3	7369.754	0.0699	3	5244.010	0.4266
	4	7124.459	0.3093	--		
	5	6987.467	0.1835	--		
	6	6842.649	0.1093	--		
	Total Peak Area: 0.9423			Total Peak Area: 0.9812		

Sample	2ν Bands (H_2O and OH)			H_2O (ν + δ) Bands		
	No. of Gaussian Peaks In Band			No. of Gaussian Peaks In Band		
	Peak	Peak Center	Peak Area	Peak	Peak Center	Peak Area
SO_4/ t-ZrO_2	1	7147.057	0.5412	1	5354.494	0.0060
	2	7116.763	1.9706	2	5264.007	0.4595
	--			3	5197.272	0.0426
	--			4	5181.609	0.7589
	Total Peak Area: 2.5118			Total Peak Area: 1.2670		

TABLE 2. The hydroxyl concentrations calculated from the diffuse reflectance spectra, given in monolayers, of monoclinic zirconia, tetragonal WO_3-impregnated zirconia, and tetragonal SO_4-impregnated zirconia.

Sample	$I_{OH(2\nu)}$	OH Conc. (monolayers)
ZrO_2	0.74607	0.18
WO_3/ZrO_2	1.34345	0.33
SO_4/ZrO_2	2.25835	0.55

Conclusions from Optical Spectroscopy. The samples have well-developed band edges, especially for the monoclinic ZrO_2 with a band edge at about 42,000 cm^{-1}. For the tetragonal SO_4/ZrO_2 catalyst, the band edge is shifted to the UV region (≈45,000 cm^{-1}), while for the tetragonal WO_3/ZrO_2 catalyst, the band edge is shifted toward the visible (VIS) region (≈35,000 cm^{-1}) and has a very large intensity with an extended tailing. The spectra can be used for diagnostics/quality control of preparation, in combination with XRD.

The NIR peaks in the 5,000-5,500 cm^{-1} region confirm the presence of water in these samples. Assignment of the NIR bands is difficult when a sample is not fully dehydrated, but the spectral shoulders below the peaks at 7159 and 7202 cm^{-1} in the tetragonal SO_4/ZrO_2 and monoclinic ZrO_2, respectively, are indicative of weakly bonded hydroxyls. A very slight shoulder is barely detectable on the peak at 7092 cm^{-1} in the tetragonal WO_3/ZrO_2 spectrum, suggesting that this sample was only partially hydroxylated.

The NIR spectra give information about sample hydroxylation. It is shown that ZrO_2 has a low degree of hydroxylation ($\approx$ 18%) and has little water of hydration associated with it. The hydroxyl concentration of the tetragonal SO_4/ZrO_2 catalyst was determined early [13] and can be used as a "benchmark". The tetragonal WO_3/ZrO_2 catalyst has weak and broad features in the hydroxyl region of the spectrum and is difficult to analysze. However, it is clear that this catalyst is less hydroxylated than the SO_4/ZrO_2 catalyst. It is noted that the WO_3/ZrO_2 catalyst has a larger electronic background in the NIR region than the other two catalysts. Quantitative analysis of the hydroxyl species in these catalysts has been carried out, but more calibration studies with reference systems are needed to achieve greater accuracy.

The UV regions of the spectra reflect electronic band-to-band transitions and show significant differences among the samples. Strong bands in the 35,000 to 48,000 cm^{-1} spectral range are observed. The spectral inflection point of tetragonal SO_4/ZrO_2 occurs at 45,000 cm^{-1}. The inflection points of the band edges of monoclinic ZrO_2 and tetragonal WO_3/ZrO_2 samples occur at about 42,225 and 34,300 cm^{-1}, respectively. In addition, the tetragonal WO_3/ZrO_2 sample shows a weak band near 25,000 cm^{-1}, while the monoclinic

ZrO_2 shows a very weak band near 32,500 cm^{-1}. These transitions giving rise to these bands can be intrepreted theoretically based on electronic structure.

XPS STUDIES OF THE ACIDITY OF WO_3/ZrO_2 AND NAFION-H CATALYSTS

This study is focusing on the diagnostics of surface acid sites to provide insight into catalyst optimization for coupling alcohols to ethers. The solid acid centers were subjected to quantitative analysis of their concentration and strength by X-ray photoelectron spectroscopy using amines as adsorbing probe molecules. The core-level N 1s photoemission exhibits a large shift towards higher binding energies upon protonation, which occurs upon interaction with Brønsted acid sites. This has been demonstrated with pyridine adsorption on Nafion-H, where the Brønsted acid sites gave rise to a N 1s peak at 401.6 eV compared with physisorbed pyridine at 398.8 eV [13]. Similarly, adsorption of pyridine on sulfated zirconia gave rise to N 1s binding energy peaks at 399.3-399.9 eV and at 401.5 eV, which were attributed to adsorption of pyridine on Lewis and Brønsted acid sites, respectively [13]. Thus, Lewis and Brønsted acid sites can be distinguished and quantified on solid acid catalysts.

For the present studies, the amines chosen were pyridine (a weak base), triethylamine (TEA, a strong base), and ethylenediamine (EDA, a bifunctional base). Survey and high resolution XPS spectral scans of the catalysts were taken before and after amine adsorption. For the zirconia samples, high resolution scans of Zr 3d, C 1s, W 4f, and N 1s regions were carried out. The $3d_{5/2}$ Zr core-level peak for clean WO_3/ZrO_2 was chosen as the reference peak for binding energy position.

A survey spectrum of the W/Z catalyst is shown in Figure 12. High resolution scans of the W 4f and Zr 3d peaks were obtained, and the observed binding energies (B.E.) and peak intensities for Zr and W are shown in Table 3 for the "clean" W/Z catalyst prior to adsorption of an amine, where FWHM is the full width at half-maximum of the peak. The peak areas were obtained by first curve-fitting the spectra using a computer program supplied with the Scienta instrument. The spectra were fitted to a Voigt function using at least 10 iterations to obtain a good fit; as defined by a "goodness-of-fit" factor based on the number of data points utilized [13]. The sensitivity factors correspond to the photoelectron cross sections that are based on theoretical calculations by Scofield [16], as tabulated in the Scienta software, but some have been refined in this laboratory by numerous practical measurements [13]. For example, the Scofield cross section for O 1s was given as 2.93, while a sensitivity factor for O 1s of 2.837 was utilized in this work. Similarly, the Scofield cross section given for N 1s was 1.80, while the sensitivity factor used in the present work was 1.62.

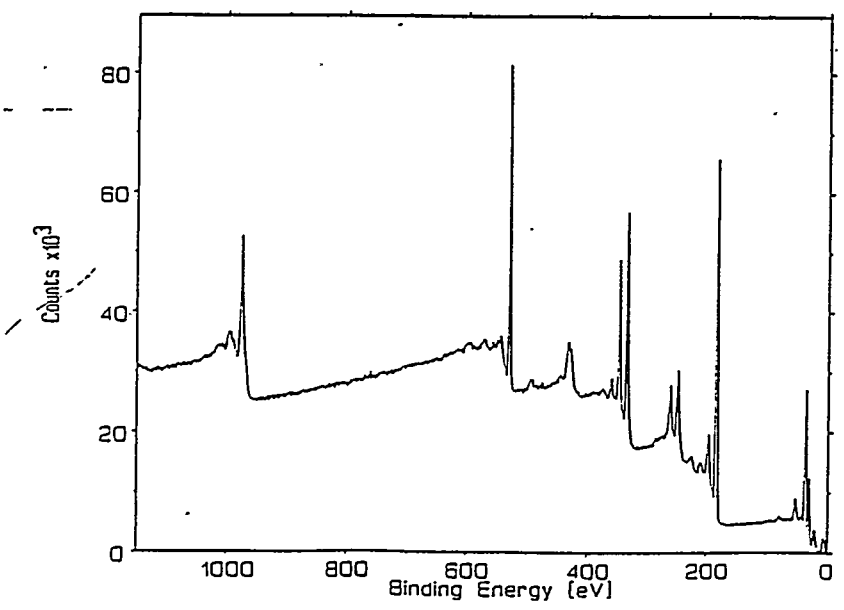

FIGURE 12. XPS survey spectrum of the W/Z catalyst.

TABLE 3. Binding energies and intensities observed for the Zr and W XPS peaks for the clean W/Z catalyst.

Peak	B.E. (eV)	FWHM (eV)	Peak Area	Sensitivity Factor	Peak Intensity
Zr $3d_{total}$	---	---	1.598×10^4	7.04	2.270×10^3
Zr $3d_{5/2}$	182.19	1.56	9.506×10^3	4.17	2.280×10^3
W $4f_{total}$	---	---	3.722×10^3	9.80	3.798×10^2
W $4f_{5/2}$	37.57	1.47	1.637×10^3	4.32	3.789×10^2
W $4f_{7/2}$	35.45	1.55	2.079×10^3	5.48	3.794×10^2

After adsorption of pyridine onto the W/Z catalyst using the procedure described in the Experimental section of this report (pp 8-10), the N 1s spectral region was scanned, and the spectrum was resolved into two peaks, as shown in Figure 13. The observed binding energies and peak intensities are given in Table 4. The pyridine adsorption indicated that most of the titrated acid sites were Brønsted acid sites, where the adsorbed pyridine had the N 1s binding energy of 401.64 eV. The presence of a N 1s peak located at lower binding energy was also indicated in the spectrum.

Similar experiments were carried out using ethylenediamine (EDA) as the adsorbing base. The resultant N 1s spectrum is shown in Figure 14. The analysis of the XPS spectral data is compiled in Table 5. It was observed that the two N 1s peaks exhibited similar intensities, indicating the presence of two N species that were approximately equal in number.

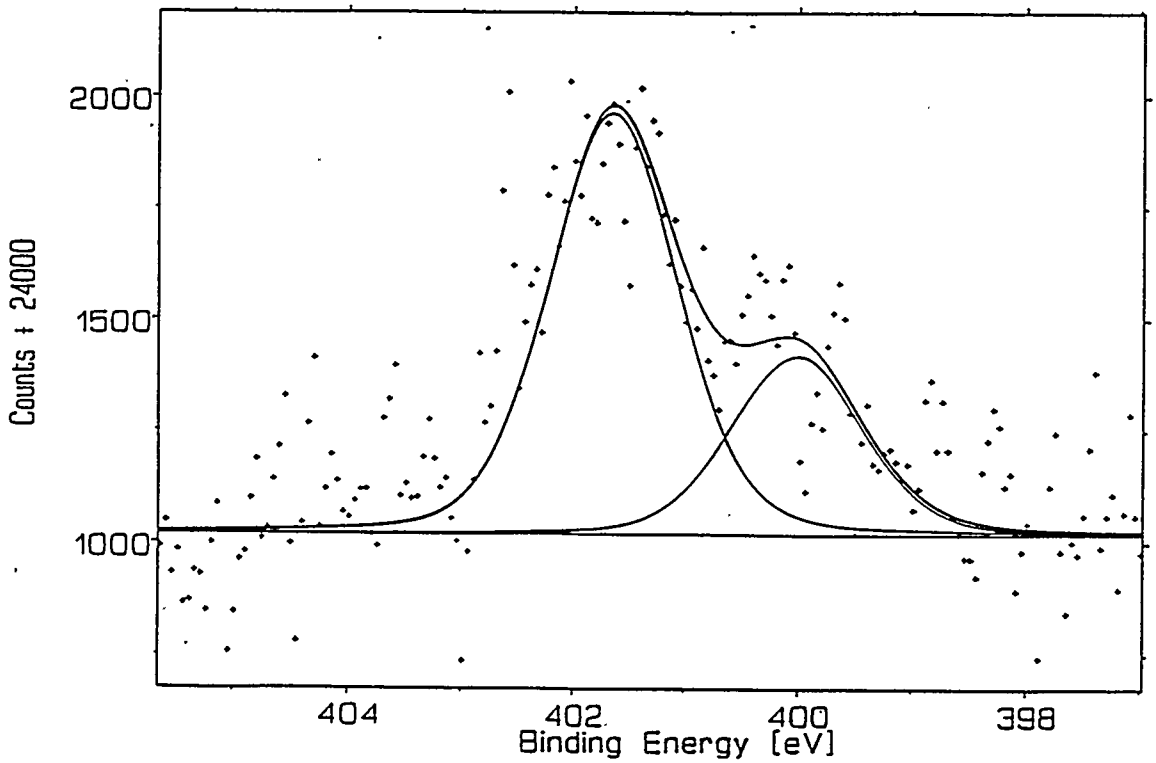

FIGURE 13. XPS spectrum of the N 1s peak for the W/Z catalyst after evacuation at 150°C, adsorption of pyridine at ambient temperature, and evacuation at 150°C. The resolved peaks (solid lines) are fitted to the experimental data points.

TABLE 4. Binding energies and intensities observed for the Zr and W peaks for the W/Z catalyst after evacuation at 150°C, adsorption of pyridine at ambient temperature, and evacuation at 150°C.

Peak	B.E. (eV)	FWHM (eV)	Peak Area	Sensitivity Factor	Peak Intensity
Zr $3d_{total}$	—	—	1.340×10^4	7.04	1.903×10^3
Zr $3d_{5/2}$	182.19	1.38	7.931×10^3	4.17	1.902×10^3
W $4f_{total}$	—	—	3.834×10^3	9.80	3.912×10^2
W $4f_{5/2}$	37.57	1.36	1.691×10^3	4.32	3.914×10^2
W $4f_{7/2}$	35.45	1.47	2.147×10^3	5.48	3.918×10^2
N $1s_{total}$	—	—	1.425×10^2	1.62	8.796×10^1
N $1s_B$	401.64	1.35	9.056×10^1	1.62	5.590×10^1
N $1s_L$	400.01	1.35	3.842×10^1	1.62	2.372×10^1

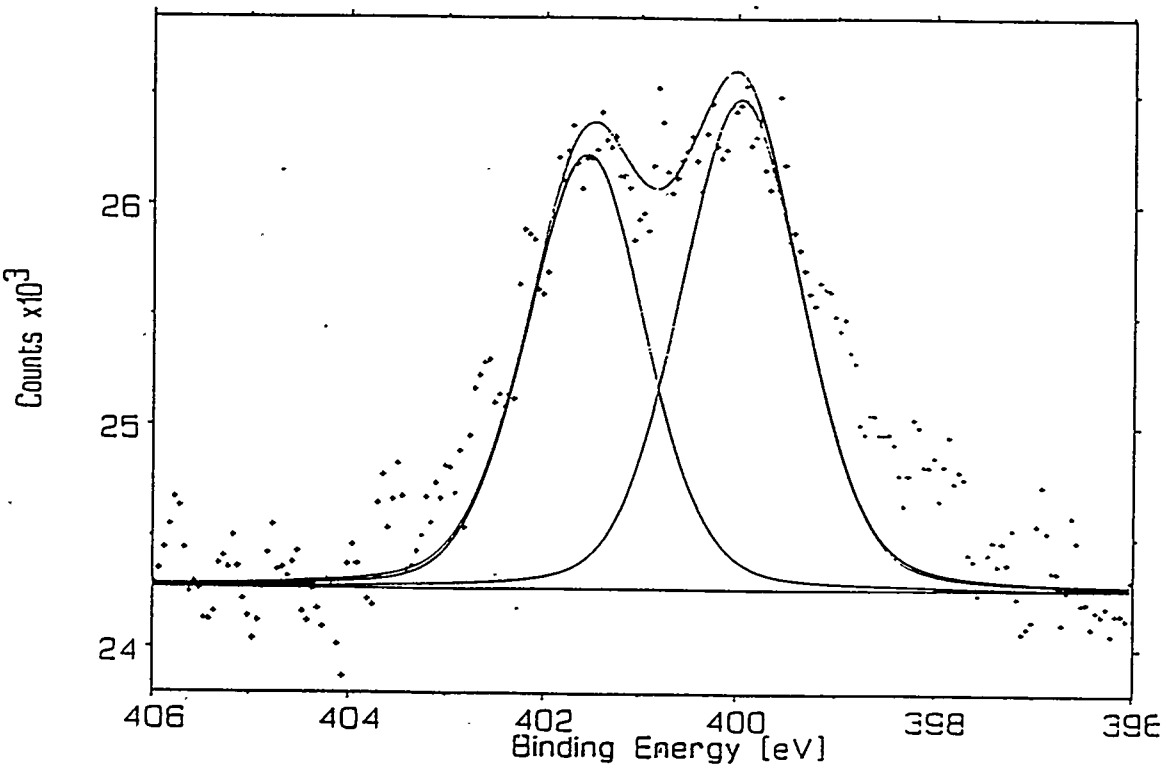

FIGURE 14. XPS spectrum of the N 1s peak for the W/Z catalyst after evacuation at 150°C, adsorption of ethylenediamine at ambient temperature, and evacuation at 150°C.

TABLE 5. Binding energies and intensities observed for the Zr and W peaks for the W/Z catalyst after evacuation at 150°C, adsorption of ethylenediamine (EDA) at ambient temperature, and evacuation at 150°C.

Peak	B.E. (eV)	FWHM (eV)	Peak Area	Sensitivity Factor	Peak Intensity
Zr $3d_{total}$	---	---	1.310×10^4	7.04	1.861×10^3
Zr $3d_{5/2}$	182.18	1.45	7.765×10^4	4.17	1.862×10^3
W $4f_{total}$	---	---	3.499×10^3	9.80	3.570×10^2
W $4f_{5/2}$	37.56	1.38	1.540×10^3	4.32	3.567×10^2
W $4f_{7/2}$	35.42	1.47	1.958×10^3	5.48	3.573×10^2
N $1s_{total}$	---	---	4.917×10^2	1.62	3.035×10^2
N $1s_B$	401.57	1.45	2.022×10^2	1.62	1.248×10^2
N $1s_L$	399.97	1.45	2.286×10^2	1.62	1.411×10^2

Similarly, triethylamine (TEA) was utilized as the absorbing nitrogen-containing base to probe the surface acid sites. The observed N 1s XPS spectrum is shown in Figure 15. Again, the spectrum was adequately fitted by two peaks. The XPS data of TEA on the W/Z catalyst are summarized in Table 6.

The **Nafion-H microsaddles** (MS) resin catalyst was also characterized by XPS analysis. Nafion-H is a fluorocarbon copolymer containing sulfonyl groups that is an insulating material and suffered charging. Therefore, a hot filament flood gun was utilized to neutralize the charging. In addition, the measured binding energies for Nafion-H samples were adjusted using the C 1s line for poly(tetrafluoroethylene) (PTFE) at 292.48 eV [17] as an internal standard. The F 1s peak for PTFE is observed at 689.67 eV [17].

The data for a clean evacuated Nafion-H MS sample are given in Table 7. Two O 1s binding energy peaks are noted. The higher binding energy peak (535.84 eV) is due to oxygen in ether linkages in the polymer backbone of the resin, while the peak at 533.31 eV corresponds to the oxygen associated with the sulfonic acid groups [10,17]. This is consistent with an O/S ratio = 3 for the sulfonic group, i.e. $-CF_2SO_3H$, where the experimental ratio from Table 7 is 2.9.

After evacuation of the Nafion-H MS sample, equilibration with ethylenediamine (EDA) was carried out, and then XPS spectra were obtained after evacuation but without heat treatment of the sample. The resultant N 1s spectrum is shown in Figure 16. The peak could correspond to the amine adsorbed on one uniform Brønsted acid site. However, the peak is slightly asymmetric, and the peak can be fitted by two Gaussians of equal intensity. The N 1s XPS data resolved for two peaks are given in Table 8.

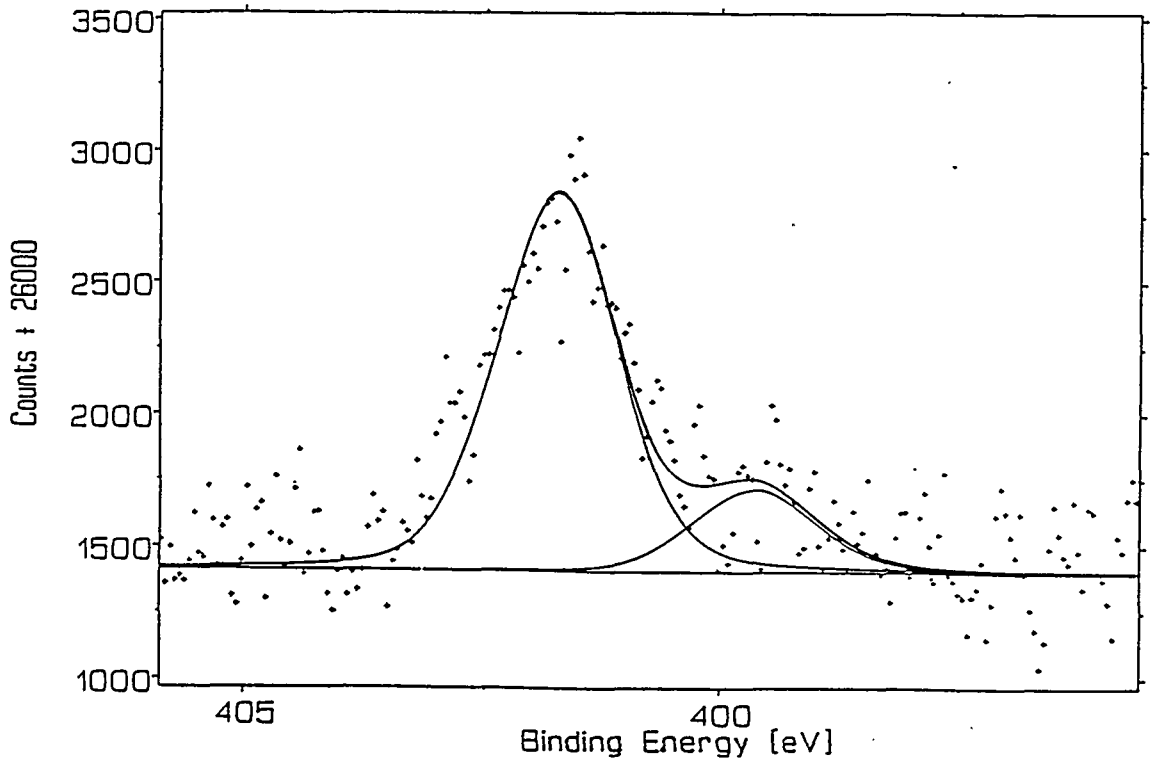

FIGURE 15. XPS spectrum of the N 1s peak for the W/Z catalyst after evacuation at 150°C, adsorption of triethylamine (TEA) at ambient temperature, and evacuation at 150°C.

TABLE 6. Binding energies and intensities observed for the Zr and W peaks for the W/Z catalyst after evacuation at 150°C, adsorption of triethylamine (TEA) at ambient temperature, and evacuation at 150°C.

Peak	B.E. (eV)	FWHM (eV)	Peak Area	Sensitivity Factor	Peak Intensity
Zr $3d_{total}$	---	---	1.511×10^4	7.04	2.146×10^3
Zr $3d_{5/2}$	182.22	1.31	8.951×10^3	4.17	2.146×10^3
W $4f_{total}$	---	---	4.370×10^3	9.80	4.459×10^2
W $4f_{5/2}$	37.66	1.31	1.930×10^3	4.32	4.467×10^2
W $4f_{7/2}$	35.51	1.28	2.450×10^3	5.48	4.471×10^2
N $1s_{total}$	---	---	2.104×10^2	1.62	1.298×10^2
N $1s_B$	401.74	1.50	1.527×10^2	1.62	9.426×10^1
N $1s_L$	399.64	1.50	3.310×10^1	1.62	2.043×10^1

TABLE 7. Binding energies and intensities observed for the clean Nafion-H MicroSaddles (MS) catalyst after evacuation.

Peak	B.E. (eV)	FWHM (eV)	Peak Area	Sensitivity Factor	Peak Intensity
F 1s	689.72	2.04	3.811×10^4	4.5880	8.306×10^3
S 2p	---	---	9.503×10^2	2.1735	4.372×10^2
$S\ 2p_{1/2}$	171.60	1.68	3.166×10^2	0.7245	4.370×10^2
$S\ 2p_{3/2}$	170.27	1.68	6.333×10^2	1.4490	4.371×10^2
$C\ 1s_{total}$	---	---	4.725×10^3	1	4.725×10^3
	294.12	1.70	8.826×10^2	1	8.826×10^2
	292.47	1.45	3.646×10^3	1	3.646×10^3
O 1s	535.84	2.50	1.970×10^3	2.837	6.944×10^2
	533.31	1.84	3.609×10^3	2.837	1.272×10^3

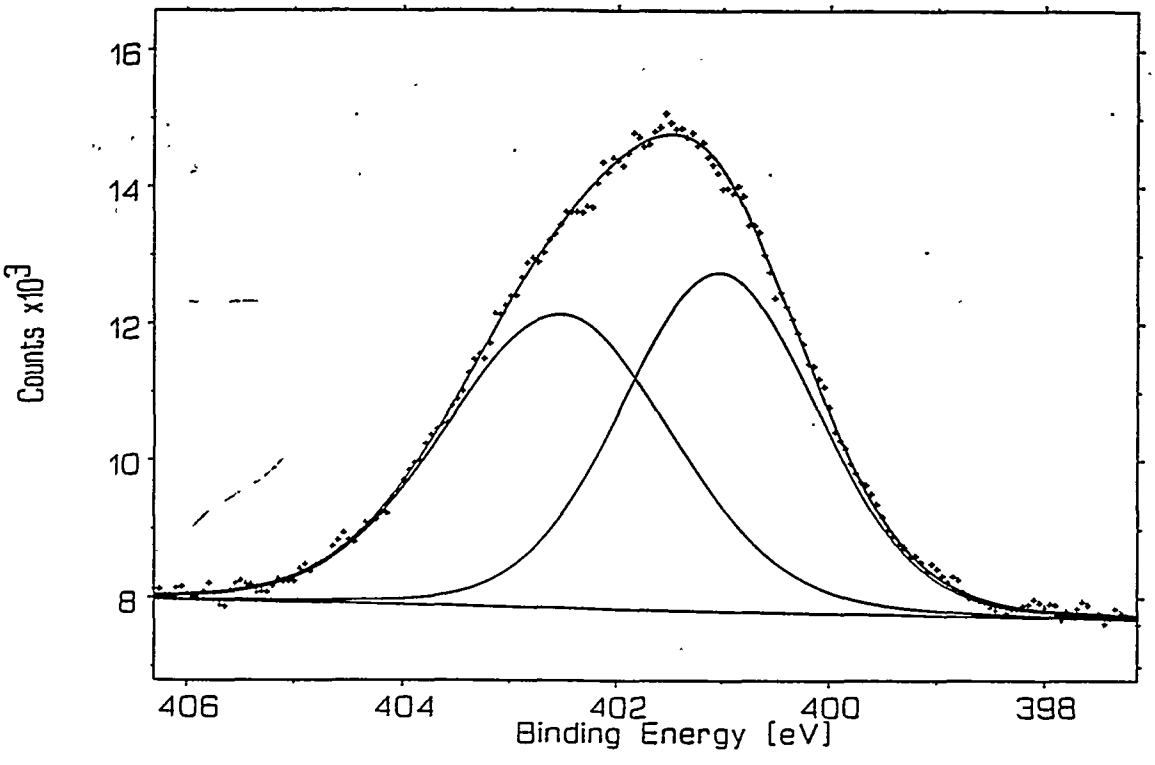

FIGURE 16. XPS N 1s spectrum of Nafion-H MS after adsorption of ethylenediamine (EDA), with no thermal post-treatment.

TABLE 8. Binding energies and intensities observed for the Nafion-H MS catalyst after adsorption of ethylenediamine (EDA), with no thermal post-treatment.

Peak	B.E. (eV)	FWHM (eV)	Peak Area	Sensitivity Factor	Peak Intensity
F 1s	689.76	2.06	4.224×10^4	4.5880	9.206×10^3
S 2p	---	---	3.379×10^2	2.1735	1.555×10^2
S $2p_{1/2}$	171.46	2.64	1.120×10^2	0.7245	1.546×10^2
S $2p_{3/2}$	170.09	2.36	2.240×10^2	1.4490	1.546×10^2
C $1s_{total}$	---	---	5.347×10^3	1	5.347×10^3
	294.09	1.82	1.360×10^3	1	1.360×10^3
	292.47	1.44	3.832×10^3	1	3.832×10^3
O 1s	536.27	2.21	1.904×10^3	2.837	6.711×10^2
	533.21	2.08	1.966×10^3	2.837	6.930×10^2
N $1s_{total}$	---	---	1.317×10^3	1.62	8.130×10^2
	402.55	2.51	6.584×10^2	1.62	4.064×10^2
	401.03	2.16	6.584×10^2	1.62	4.064×10^2

The Nafion-H MS sample with the adsorbed ethylenediamine (EDA) was subsequently evaculated while being heated at 150°C. The sample was then analyzed again by XPS at ambient temperature, and the resultant N 1s spectrum is shown in Figure 17. The top of the peak appears to be flatter, and the peak can again be resolved into two peaks of equal intensity. The analysis of the XPS data is tabulated in Table 9.

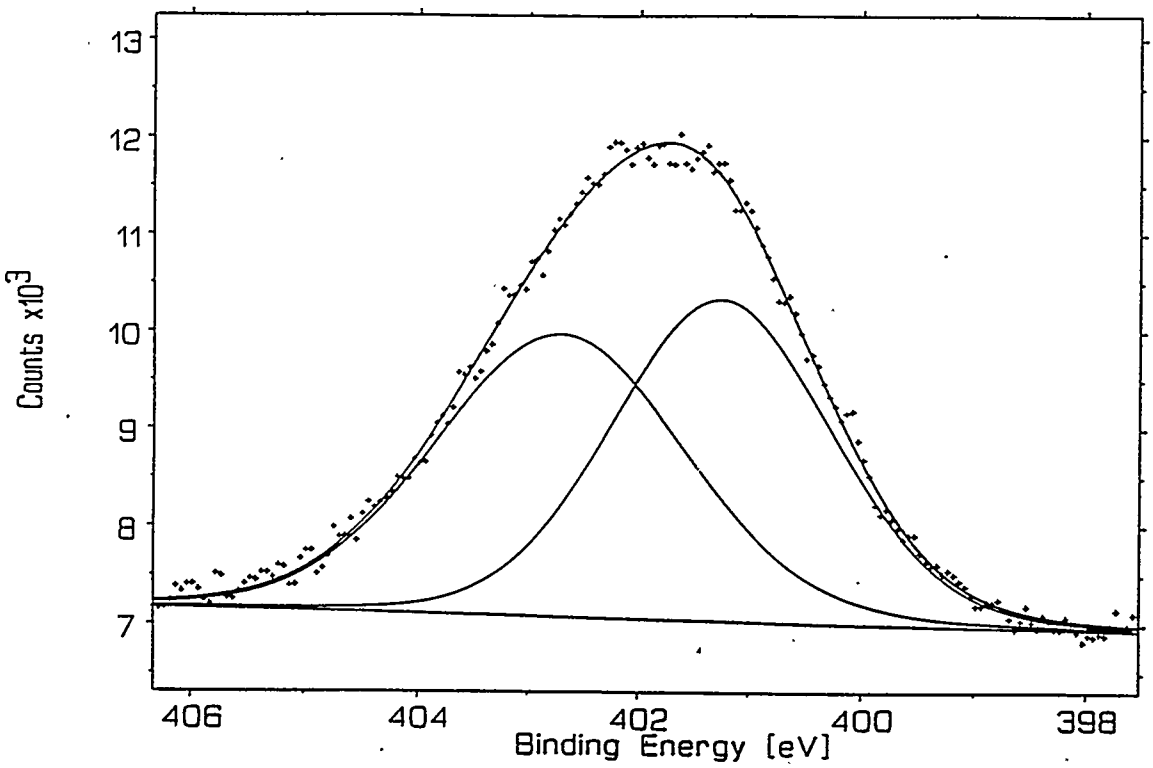

FIGURE 17. XPS N 1s spectrum of Nafion-H MS after adsorption of ethylenediamine (EDA), followed by a thermal post-treatment at 150°C.

As shown, the titration of acid sites gives different results with the different amines. Pyridine titrates 13% of the Brønsted acid sites, while TEA, a strong base that could be sterically hindered on the surface, titrates 22% of the acid sites. EDA titrates 37% of the Brønsted acid sites. Therefore, the accessibility of the Brønsted acid sites on W/Z follows the order of EDA > TEA > pyridine, while the basicity of the amines follows the order TEA > EDA > pyridine. The tungstated zirconia ia not the same as the sulfated zirconia (S/Z). With the latter catalyst, pyridine titrates all Brønsted acid sites, while that is not the case with the tungstated zirconia.

TABLE 9. Binding energies and intensities observed for the Nafion-H MS catalyst after adsorption of ethylenediamine (EDA), followed by thermal post-treatment of evacuation at 150°C.

Peak	B.E. (eV)	FWHM (eV)	Peak Area	Sensitivity Factor	Peak Intensity
F 1s	689.74	2.16	4.265×10^4	4.5880	9.296×10^3
S 2p	---	---	2.709×10^2	2.1735	1.206×10^2
$S\ 2p_{1/2}$	171.75	2.64	9.046×10^1	0.7245	1.249×10^2
$S\ 2p_{3/2}$	170.26	2.36	1.809×10^2	1.4490	1.248×10^2
$C\ 1s_{total}$	---	---	5.581×10^3	1	5.581×10^3
	294.09	1.82	1.716×10^3	1	1.716×10^3
	292.47	1.44	3.693×10^3	1	3.693×10^3
O 1s	536.22	2.21	2.008×10^3	2.837	7.078×10^2
	533.26	2.08	1.496×10^3	2.837	5.273×10^2
$N\ 1s_{total}$	---	---	9.404×10^2	1.62	5.805×10^2
	402.71	2.51	4.701×10^2	1.62	2.902×10^2
	401.26	2.16	4.701×10^2	1.62	2.902×10^2

It is concluded from this study that the amine bases titrate the Brønsted acid sites on these acid catalysts. However, the surface concentration of the accessible acid sites on the tungstena/zirconia catalyst is lower than expected from the tungstate content and are more diluted than observed with the Nafion-H catalyst. In addition, the Brønsted acid sites on the tungstena/zirconia catalyst are heterogeneous since stronger amine bases detect more acid sites.

MODELLING OF ETHER SYNTHESIS OVER NAFION-H

Kinetic results suggest that the mechanism of the ether-forming reaction on WZ is the same as on SZ and Nafion-H. We are examining the dual-site S_N2 reaction pathway theoretically *via ab initio* DFT (BP86, DN**) calculations [18] of the prototype system 2S + M + B (S ≡ CF_3SO_3H, M ≡ CH_3OH, B ≡ $(CH_3)_2CHCH_2OH$). These computations are being extended to DME synthesis for comparison.

Geometries have been optimized and true global minima have been found. The transition state (TS) has been found that satisfies the criteria of one imaginary frequency with root mean square gradient of 0.00023 hartree/Å. The calculated total energies are ΔE(S) = −962.4218, ΔE(M) = −115.7793, and ΔE(B) = −194.4431 hartrees, respectively, and energy differences on the reaction pathway are given in Table 10.

The calculated energies for MIBE synthesis are shown in Table 10, and the results demonstrate that:

(1) the TS barrier from free reactants, $E^{\ddagger} \cong 16$ kcal/mol, is comparable to the experimental 15 kcal/mol obtained with Nafion-H [6,14],

(2) the overall reaction is nearly thermally neutral ($E_{(reaction)} \cong -6$ kcal/mol), in agreement with thermochemical data (ΔH = −5.53 kcal/mol) [14],

(3) sorbed intermediates involve hydrogen-bonded methanol and more strongly held hydrogen-bonded isobutanol, in agreement with the pattern derived from kinetic data [6],

(4) MIBE is more weakly bonded than the precursor alcohols but H_2O is more strongly held, and

(5) weak (≈4 kcal/mol) cooperative complex formation between the sorbed methanol and isobutanol reactants or the sorbed products is predicted.

Table 10. Energetics of the dual-site S_N2 pathway M + B → TS → MIBE + W over sulfonic acid sites.[a]

1	2		3	4	5	6		7
	2a	2b				6a	6b	
M + B + 2S	M | S	B | S	M·····B ⋮ ⋮ S·····S	TS	MIBE····W ⋮ ⋮ S·····S	MIBE ⋮ S	W ⋮ S	MIBE + W + 2S
0	−14.81	−13.68	−22.44	−6.63	−28.58	−12.53	−10.92	−1.44

[a]All energies are in kcal/mol, DFT (BP86, DN**) optimized. M ≡ CH_3OH, B ≡ $(CH_3)_2CHCH_2OH$, MIBE ≡ $(CH_3)_2CHCH_2OCH_3$, W ≡ H_2O, S ≡ CF_3SO_3H, and TS ≡ the transition state. The columns represent:

1. Separated alcohol reactants and two acid sites;
2. Alcohols adsorbed on two separate acid sites;
3. Sorbed precursor complex of alcohols and two proximal acid sites;
4. Transition state;
5. Sorbed complex of product MIBE and water on two proximal acid sites;
6. MIBE and water adsorbed on two separate acid sites; and
7. Separated products and two acid sites.

The above features, in conjunction with experimental results, suggest a pathway in which the alcohols are brought together by hydrogen bonding to the proximal sites and the sorption complexes are transformed into the TS by a concerted methyl transfer between the two alcohol oxygens and three protons transfer among the methanol and two sulfonic groups.

The TS structure is shown in Figure 18 with two pathway-driving orbitals involving the carbon C_o of the CH_3 group of MeOH. The i-BuO(H)····CH_3····OH_2 angle is 175.3° and the CH_3 group is planar as the configuration of the H atoms is being inverted from that in

MeOH to that in MIBE. The σ-TS orbital (Figure 18A; -32.33 hartree) connects the two Os adjacent to CH_3 as O 2pσ-C 2s-O 2pσ, and the π-TS orbital (Figure 18B; -18.56 hartree) as O 2pπ-C 2pπ-O 2pπ in an antarafacial fashion. These orbitals are nearly symmetric and are very sensitive to the movement of the CH_3 toward one O or another, tantamount to breaking one C-O bond and strengthening the other.

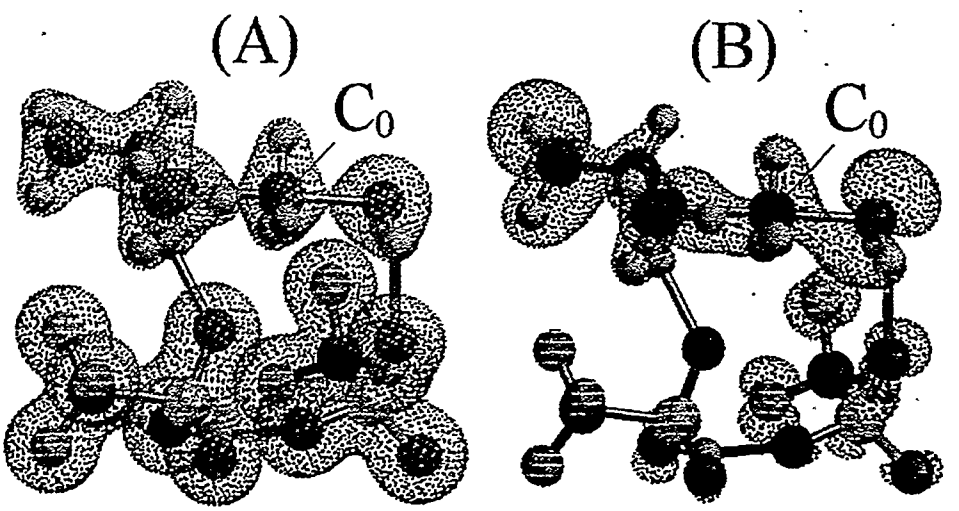

Figure 18. The dual site TS structure for the MeOH + i-BuOH → MIBE + H_2O reaction pathway showing **(A)** the σ-TS orbital and **(B)** the π-TS orbital as the methyl group of MeOH moves toward forming the ether linkage. The atoms represented by colors are: red for O, gray for H, black for C, green for F, and blue for S.

Sulfated zirconia and tungstated zirconia have been established as very strong acids [9,13], as have the fluorocarbon sulfonic acids [1,14]. Furthermore, evidence based on hydrocarbon isomerizations indicates that WO_3/ZrO_2 possesses stronger acid sites than SO_4/ZrO_2 [9]. We have herein quantified at the DFT/BP/DN** level [19] the relative acidities of SO_4/ZrO_2 and CF_3SO_3H and the basicities of pyridine and ethylenediamine (EDA) by calculating acid-base interaction energies. Reactants and products were fully

optimized to rms gradient <0.0005 hartree/Å. The SO_4/ZrO_2 catalyst site was modeled as $(HO)_3ZrOSO_3H$. The interaction energies are summarized in Table 11, which show that (1) SO_4/ZrO_2 (SZ) is a slightly stronger acid than CF_3SO_3H by 1.3-1.4 kcal/mol, (2) EDA is a stronger base than pyridine by 4.1-4.2 kcal/mol, and (3) the SO-H and H-N distances reflect the strength of the acid-base interaction.

Table 11. Energies (kcal/mol) of acid-base interactions and the SO-H-N distances (Å)[a] derived from the computational models.

	BASE	
ACID	Pyridine	EDA
SZ	-18.54 (1.49, 1.10)	-22.72 (1.52, 1.09_6)
CH_3SO_3H	-17.23 (1.37, 1.16)	-21.29 (1.67, 1.07)
$(CH_3SO_3H)_2$[b]	-------	-21.61 (3.87, 1.04)[d]
$(CH_3SO_3H)_2$[c]	-------	-33.69 (1.12, 1.44)[e]

[a]Entries in parentheses are the (SO-H distance, H-N distance) involving hydrogen between the SO- and -N= groups;
[b]EDA bound with one nitrogen to the acid group with hydrogen transfer;
[c]EDA bonded symmetrically to both acid groups;
[d]Only one of the two nitrogens is a proton acceptor; and
[e]Both nitrogens are bonded

CONCLUSIONS

With respect to the WO_3/ZrO_2 catalyst under investigation in this research, the following conclusions can be made:

1. The tungstena/zirconia catalyst is active for coupling methanol and isobutanol to methylisobutylether (MIBE), but sideproducts are formed that consist mainly of isobutene, octenes, and dimethylether.
2. When the reaction temperature is increased above 135°C, the stable tungstena/zirconia catalyst is very good for dehydration of isobutanol to isobutene, even in the presence of methanol.
3. Ether and isobutene synthesis over the tungstena/zirconia catalyst could be described by Langmuir-Hinshelwood kinetics in which competitive adsorption of the two alcohols on surface Brønsted acid sites is a dominant feature and is consistent with a dual-site mechanism, similar to that previously described with Nafion-H [1,6], that proceeds *via* a S_N2 pathway.
4. The surface concentration of the accessible acid sites on the tungstena/zirconia catalyst is lower than expected from the tungstate content and are more diluted than observed with the Nafion-H catalyst.
5. The Brønsted acid sites on the tungstena/zirconia catalyst are heterogeneous since stronger amine bases detect (titrate) more Brønsted acid sites.
6. From the modelling study with the prototype sulfonic acid moiety, it is shown that the transition state barrier from the free reactants, ≈16 kcal/mol, is comparable to the experimental 15 kcal/mol obtained with the Nafion-H resin [1,14].

REFERENCES

1. K. Klier, A. Beretta, Q. Sun, O. C. Feeley, and R. G. Herman, Catal. Today, **36** (1997) 3.

2. K. Klier, Q. Sun, O. C. Feeley, M. Johansson, and R. G. Herman, in *"Proc. 11th Intern. Congr. Catal.-40th Ann.,"* (Studies in Surface Science and Catalysis), **101A**, ed. by J.W. Hightower, W.N. Delgass, E. Iglesia, and A.T. Bell, Elsevier, Amsterdam, 601 (1996).

3. L. Lietti, Q. Sun, R. G. Herman, and K. Klier, Catal. Today, **27** (1996) 151.

4. O. C. Feeley, Q. Sun, R. G. Herman, M. Johansson, L. Lietti, and K. Klier, Catal. Letters, **35** (1995) 13.

5. Q. Sun, R. G. Herman, and K. Klier, J. Chem. Soc., Chem. Commun., (1995) 1849.

6. J. G. Nunan, K. Klier, and R. G. Herman, J. Catal., **139** (1993) 406.

7. R. G. Herman, K. Klier, O. C. Feeley, and M. A. Johansson. Preprints, Div. Fuel Chem., ACS, **39(2)** (1994) 343.

8. J. Nunan, K. Klier, and R. G. Herman, J. Chem. Soc., Chem. Commun., (1985) 676.

9. J. G. Santiesteban, J. C. Vartuli, S. Han, R. D. Bastian, and C. D. Chang, J. Catal., **168** (1997) 431.

10. K. Klier, Catal. Rev., **1** (1967) 207.

11. G. F. A. Korteum, *"Reflectance Spectroscopy; Principles, Methods, Applications,"* Engl. Translation by J. E. Lohr, Springer, NY (1969).

12. K. Klier, J. Opt. Soc. Am., **62** (1972) 882.

13. M. Johansson and K. Klier, Topics Catal., **4** (1997) 99; M. Johansson, Ph.D. Dissertation, Department of Chemistry, Lehigh University (1995).

14. K. Klier, R. G. Herman, R. D. Bastian, S. DeTavernier, M. Johansson, M. Kieke, and O. C. Feeley, in *"Proc. Liquefaction Contractors' Review Meeting, U.S. Department of Engery-PETC,"* ed. by G. J. Stiegel and R. D. Srivastava, Pittburgh, PA, 20-49 (1991).

15. J. H. Shen and K. Klier, J. Phys. Chem., **84** (1980) 1453.

16. J. H. Scofield, J. Electron Spectrosc. Relat. Phenom., **8** (1976) 129.

17. G. Beamson and D. Briggs, "*High Resolution XPS of Organic Polymers: The Scienta ESCA Database*," Wiley and Sons, Chichester, England (1992).

18. SPARTAN, ver. 3.1, Wavefunction, Inc., Irvine, CA, USA.

19. The DN** basis set uses polarization functions for hydrogen, is equivalent in performance to Gaussian 6-311G**, and its construction follows that in B. Delley, J. Chem. Phys., **92** (1990) 508 (Wavefunction, Inc., private communication).